Spring 2019

Magnesium-rich Phyllosilicates in Creeping Faults: A Study of the Maacama Fault Zone, Mendocino County, California

Brittany M. Martin
San Jose State University

MAGNESIUM-RICH PHYLLOSILICATES IN CREEPING FAULTS: A STUDY OF THE MAACAMA FAULT ZONE, MENDOCINO COUNTY, CALIFORNIA

A Thesis

Presented to

The Faculty of the Department of Geology

San José State University

In Partial Fulfillment

of the Requirements for the Degree

Master of Science

by

Brittany Martin

May 2019

The Designated Thesis Committee Approves the Thesis Titled

MAGNESIUM-RICH PHYLLOSILICATES IN CREEPING FAULTS: A STUDY OF THE MAACAMA FAULT ZONE, MENDOCINO COUNTY, CALIFORNIA

by

Brittany Martin

APPROVED FOR THE DEPARTMENT OF GEOLOGY

SAN JOSÉ STATE UNIVERSITY

May 2019

Kimberly Blisniuk, Ph.D.	Department of Geology
Jonathan Miller, Ph.D.	Department of Geology
Ellen Metzger, Ph. D.	Department of Geology

ABSTRACT

MAGNESIUM-RICH PHYLLOSILICATES IN CREEPING FAULTS: A STUDY OF THE MAACAMA FAULT ZONE, MENDOCINO COUNTY, CALIFORNIA

by Brittany Martin

The Maacama Fault Zone in Mendocino County, California consists of multiple fault gouges with varying mineralogy, making this an ideal location to study the potential relationship between the magnesium phyllosilicate content of a fault gouge and fault creep. This study uses the presence of magnesium-rich phyllosilicates to test the hypothesis that faults to the northeast of Little Lake Valley in Mendocino County are accommodating strain on the Maacama Fault Zone through creep. Analytical work expands the work of Schroeder (2010) to more completely address the relationship between fault creep and mineralogy by sampling three fault gouges in the Maacama Fault Zone. The mineralogical content and textures of these gouges were characterized using petrographic analysis, x-ray diffraction, and scanning electron/energy dispersive spectrometry. Corrensite, a chlorite-smectite interlayer clay that has been found in creeping faults, was found within one of the fault gouges, along with chlorite, suggesting aseismic activity may be present on these faults.

ACKNOWLEDGMENTS

This Master's Thesis could not have been completed without the support of my husband, Troy Martin, and my children, Leif, Ryle, and Gretel Martin. They endured two years of commuting at early hours in the morning, arriving home late at night, weekends on field trips, and evenings studying for exams and writing. Troy helped with getting children and shuffling them to sporting events, to and from school, and to and from daycare. My kids encouraged me even when they had early morning wake-up calls to help and walking home alone.

Thanks also to my employer, St. Abraham's Classical Christian Academy in Aptos, California. My headmaster continually worked my teaching schedule around my classes and the time that I needed for writing.

Thanks to my advisor, Dr. Ellen Metzger, who helped me find a topic which was interesting to me and relevant to our region.

Thanks to Diane Moore for her input regarding my work, and to the U.S. Geological Survey in Menlo Park for generous use of their analytical equipment.

Lastly, my thanks goes out to the retired Oakland teachers who let me access their private property to map these faults. After owning the property for 20 years they were more than generous with their property, their time, and their knowledge of the region. Being native Californians, they also had no problem with active faults in their back yard.

TABLE OF CONTENTS

LIST OF TABLES

LIST OF FIGURES

INTRODUCTION

The relationship between phyllosilicate-rich fault gouges and fault creep has been well documented in recent years (e.g. Tesei et al., 2012; Janssen et al., 2014; Moore, 2014; Schleicher et al., 2015; Harris, 2017). Creeping faults often contain an array of magnesium-rich clays including talc, saponite, and corrensite that form within the fault zone (Haines and van der Pluijm, 2012; Schleicher et al., 2012, 2015; Tesei et al., 2012; Moore, 2014). Due to circulating fluids in the fault gouge, dissolution-precipitation reactions cause the alteration of mafic and ultramafic minerals, which generates a wide variety of smectite clays, including corrensite (Moore and Rymer, 2012; Schleicher et al., 2012; Janssen et al., 2014; Moore, 2014; Schleicher et al., 2015). Many studies looking into a mineralogical basis for fault creep have focused on faults within the San Andreas Fault System (SAFS) of California (Moore and Rymer, 2012; Schleicher et al., 2012; Moore and Lockner, 2013; Moore, 2014).

The Maacama Fault Zone (MFZ) lies in northern Napa and Mendocino Counties, California and is one of the northernmost fault zones of the San Andreas Fault System (SAFS) (Figure 1). The MFZ contains multiple creeping faults and cuts through Central Belt Franciscan Assemblage blocks, making it mineralogically similar to creeping sections of the SAFS (Woolace, 2005; Moore, 2014; Murray et al. 2014). The identification of multiple creeping faults in the MFZ has implications for the overall seismic hazard of this region (Prentice et al., 2014). Erickson (2008) identified multiple faults of the MFZ in and around Little

Lake Valley in Mendocino County, California (Figure 2). She argued that these faults were regionally linked to the main trace of the Maacama Fault in a developing flower structure. Schroeder (2010) identified multiple faults within the MFZ to the northeast of Little Lake Valley, and used mineralogical content to support the idea that these faults were creeping.

The purpose of this study is to evaluate aseismic activity on the MFZ by identifying faults to the northeast of Little Lake Valley (LLV) in Mendocino County. This study extends Schroeder's (2010) description of lithology and mineralogy that characterized fault gouges of the MFZ (Figure 2). Fault gouge mineralogy is described, with a particular focus on magnesium-rich phyllosilicates. Samples were taken in a transect across fault gouges from two locations identified by Schroeder (2010), and an additional site located nearby. Thin sections were made of the gouge material. Petrography, x-ray diffraction analysis, and scanning electron microscopy with electron dispersive spectroscopy were used to characterize the textures and minerals present within the gouge. Based on fault gouge mineralogy, my hypothesis is that this region of the MFZ is creeping, helping to accommodate strain on the overall fault zone. Fault gouges rich in magnesium-rich phyllosilicate smectite clays, such as corrensite, will be an indicator of this activity.

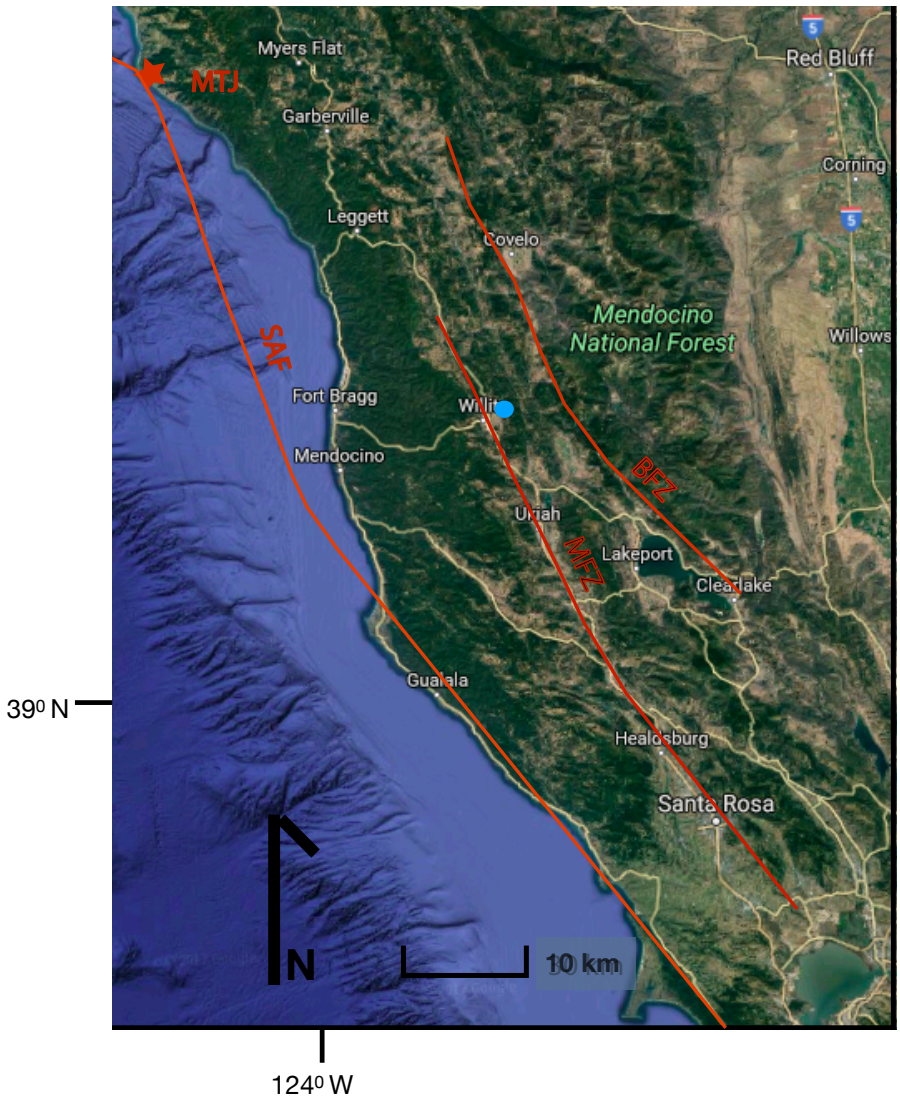

Figure 1: The location of the Maacama Fault Zone (MFZ) in relationship to the San Andreas Fault System (SAF) and Bartlett Springs Fault Zone (BFZ) in Northern California. Location of the Mendocino Triple Junction (MTJ) is also noted. Blue dot indicates location of this study.

BACKGROUND

The Maacama Fault Zone

Movement between the Pacific and North American plates in California is accommodated by an array of fault zones within the SAFS, a 100-km wide fracture zone striking north to south through California (e.g. Herd, 1978; Bilham and Bodin, 1992; Murray et al., 2014). Large fault systems accommodate the movement between tectonic plates, which include the Pacific and North American Plates in California (e.g. Herd, 1978; Bradbury et al., 2007). The SAFS includes the main trace of other faults as well as their surrounding damage zones (e.g. Herd, 1978; Bradbury et al., 2007; Murray et al., 2014). In northern California, these zones consist of large segments of right-stepping, right-lateral strike-slip fault zones extending north from Hollister, California to the continental shelf off the coast of Crescent City, California (e.g. Herd, 1978; McLaughlin et al., 1988). North of Santa Rosa, these fault zones run sub-parallel to the SAFS and include the Rodger's Creek Fault Zone, the Maacama Fault Zone (MFZ) and the Bartlett Springs Fault Zone (Figure 1) (Erickson, 2008). A 5-kilometer right-stepping segment separates the northern end of the main trace of Rodgers Creek Fault from the southern tip of the main trace of the Maacama Fault in Sonoma County, north of Santa Rosa (Herd, 1978; Murray et al., 2014). From that point, the MFZ runs north for 110-160 km into Mendocino County (e.g. Herd, 1978; Bilham and Bodin, 1992; Schroeder, 2010; Murray et al., 2014).

The MFZ cuts through rocks of the Central Belt Franciscan Complex, which is metamorphosed to the zeolite facies and characterized by the presence of greenstone, greywacke, serpentinite, and blueschist (McLaughlin, 1988; Woolace, 2005; Schroeder, 2010; Prentice et al., 2014). In central Mendocino County, the MFZ consists of the main trace of the Maacama Fault, as well as multiple en echelon faults within a 5-6 km-wide damage zone (Woolace, 2005; Erickson, 2008). The main trace of the Maacama Fault runs through the town of Willits, while the rest of the damage zone runs east across a wide, intermontane basin known as Little Lake Valley (LLV) (Figure 2) (Woolace, 2005; Erickson, 2008). LLV is bounded both on the southeast and northeast by the East Willits Fault, while the damage zone continues east another 2-3 km (Erickson, 2008; Schroeder, 2010).

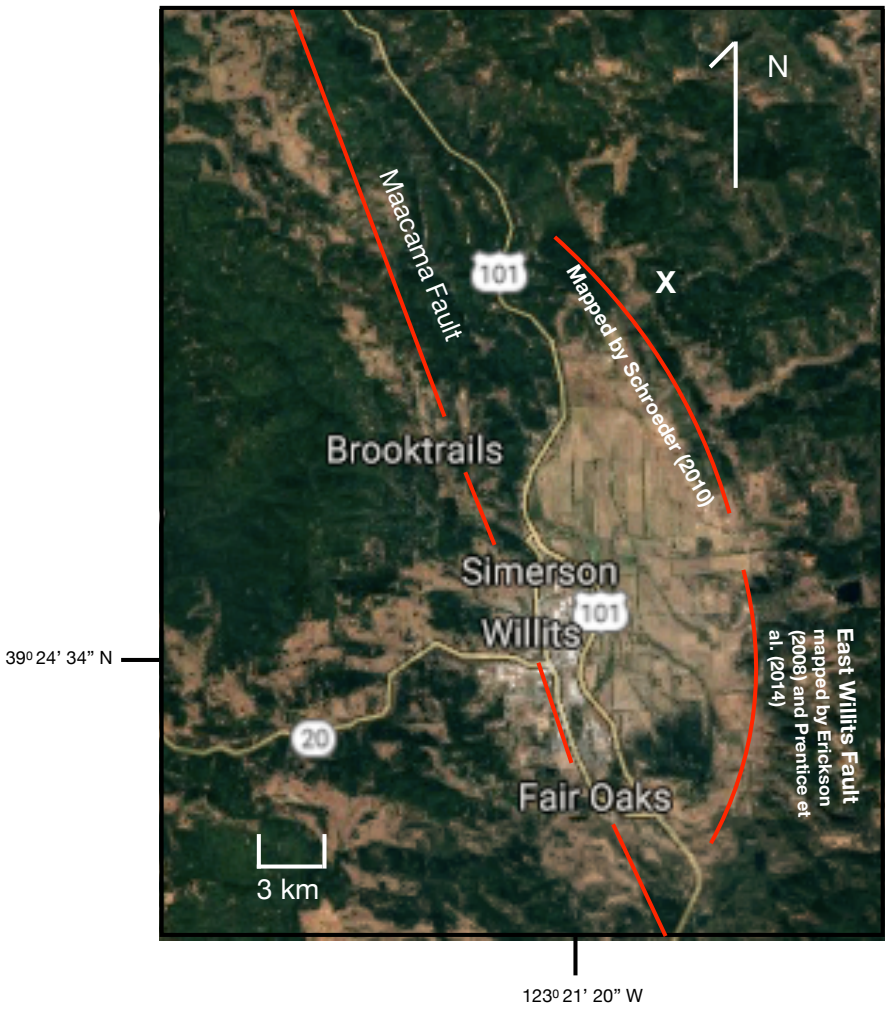

Figure 2: Little Lake Valley, east of Willits, California. Erickson (2008) identified a fault to the east of the valley, naming it the East Valley Fault. Schroeder (2010) argued that a faults to the north of the East Valley Fault constitute a continuation of that structure. Prentice et al. (2014) re-named this structure the East Willits Fault. Location of this study marked by the "X."

Previous Work

Both seismic and aseismic movement on the MFZ are well documented. Current activity of the faults east of LLV have only began to be studied, but seismic activity around LLV in the form of magnitude 2-3 earthquakes has been recorded over the past 30 years (Erickson, 2008; Schroeder, 2010). Erickson (2008) argued that the MFZ uses pre-existing fabric within the Franciscan melange to accommodate strain, and mapped two different faults to the east of LLV, naming the entire structure the East Valley Fault. She also took geophysical measurements indicating that the MFZ is a developing, upward-facing flower structure centered under LLV. This recent structure has new faults coming to the surface over time (Erickson, 2008). Prentice et al. (2014) re-named this structure the East Willits Fault (Figure 2).

The slip rate for the MFZ has been determined both geodetically by GPS and geologically from trench studies. The geodetic slip rate for the MFZ is 13.1 ± 0.8 mm/yr, while the geologic slip rate measured on the main trace of the Maacama Fault is 6.4-8.6 mm/yr (Murray et al., 2014; Prentice et al., 2014). Sedimentary trench studies of offset stream beds in LLV indicate that this section of the fault has experienced stable movement for the past 50-700 years (Woolace, 2005; Prentice et al., 2014). The creep rate, as determined by various alignment arrays, is 3.3 ± 4.3 mm/yr on the northern portion of the Rodger's Creek Fault Zone, which is connected at depth to the MFZ (Funning et al., 2007; Murray et al., 2014). Along the main trace of the Maacama Fault, through the town of

Willits, the creep rate ranges from 5.7-6.5 mm/yr, which is one of the highest rates for any northern California strike-slip fault (Galehouse and Lienkaemper, 2003; Prentice et al., 2014). These values are summarized in Table 1, showing a significant slip deficit between the geodetic slip rate and the geologic slip and creep rates. Prentice et al. (2014) hypothesized that either strain is increasing within the MFZ, indicating the possibility of a future large earthquake, or other structures in the region may be accommodating strain.

Table 1: Summary of slip and creep rates measured on the MFZ near Willits, CA.

	mm/yr	**Reference**
Geodetic Slip Rate	13.7 13.1 ± 0.8	Erickson, 2008 Murray et al., 2014
Geologic Slip Rate	5 6.4-8.6	Woolace, 2005 Prentice et al., 2014
Creep Rate	3.3 ± 4.3 6.5 5.7 ± 0.01	Funning et al., 2007 Galehouse & Lienkaemper, 2003 Prentice et al., 2014

Schroeder (2010) identified multiple faults to the northeast of LLV, and mapped them as a northern continuation of the East Willits Fault (Figure 2). Geomorphic evidence suggests that these faults have experienced recent movement, as noted by their association with several Pleistocene landslides (Schroeder, 2010). In two fault gouges northeast of LLV, Schroeder (2010) found serpentine minerals in juxtaposition with quartzofeldspathic rocks, similar to what has been observed along creeping sections of the SAFS at the San Andreas Fault Observatory at Depth (SAFOD) (Schleicher et al., 2012; Moore, 2014).

Schroeder (2010) used geophysical measurements to determine that seismogenic clusters beneath LLV coincide with serpentinite lenses, which was later confirmed with well core data. Based on the mineralogical similarity to the environment observed at the SAFOD, Schroeder (2010) concluded that the faults northeast of LLV are creeping.

In this thesis, the work of Schroeder (2010) is extended by examining and characterizing fault gouge mineralogy of three gouges within the MFZ to the northeast of LLV, in order to identify potentially creeping faults that may accommodate strain in the fault zone. This study will focus particularly on magnesium-rich phyllosilicates, using x-ray diffraction and energy dispersive spectrometry to characterize the clay minerals found within these gouges.

Magnesium-rich Clays

Structure

Magnesium-rich phyllosilicates include the serpentine polymorphs and chlorite, as well as the saponite clays (e.g. Moore and Rymer, 2007; Tesei et al., 2012). The clays are made of tetrahedral layers where silicon and aluminum are bonded with oxygen, and octahedral layers that contain aluminum, magnesium, and iron cations surrounded by oxygen and hydroxyls (Brigatti et al., 2013, Evans et al., 2013). Clays are classified as 2:1 layer clays when their structure contains 2 tetrahedral layers and 1 octahedral layer (Brigatti et al., 2013) (Figure 3). Clay structures with all 6 octahedral sites occupied by cations are designated as trioctahedral clays (Brigatti et al., 2013). In the magnesium-rich phyllosilicates, a high proportion of these cations are magnesium and iron (e.g. Brigatti et al., 2013; Schleicher et al., 2015). These phases include chlorite and the smectite clays, including corrensite (e.g. Schleicher, 2012; Moore, 2014). Additionally, trioctahedral clays that contain water between their layers are known as the trioctahedral expanding clays (Shau et al., 1990; Moore and Lockner, 2007). When heated, these clays will release their water layers, causing them to expand (Moore and Rymer, 2007). Figure 4 shows the structural relationship between chlorite and a trioctahedral expanding clay, such as a smectite clay. Water molecules and exchangeable cations calcium (Ca^{2+}), magnesium (Mg^{2+}), sodium (Na^{+}), and potassium (K^{+}) occur between T-O-T packets, which are joined by weak van der Waals bonds (Shau et al., 1990; Brigatti et al., 2013).

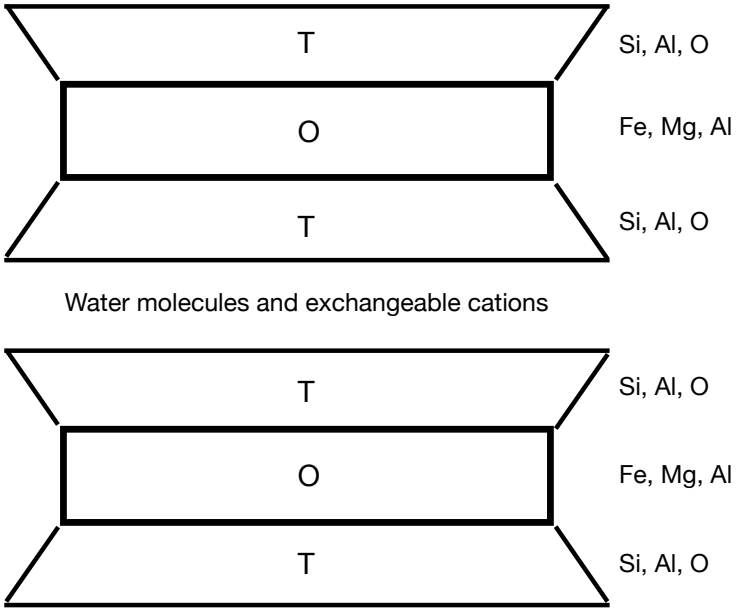

Figure 3: Relationship of tetrahedral (T) and octahedral (O) layers in 2:1 layer clays (modified from Shau et al., 1990).

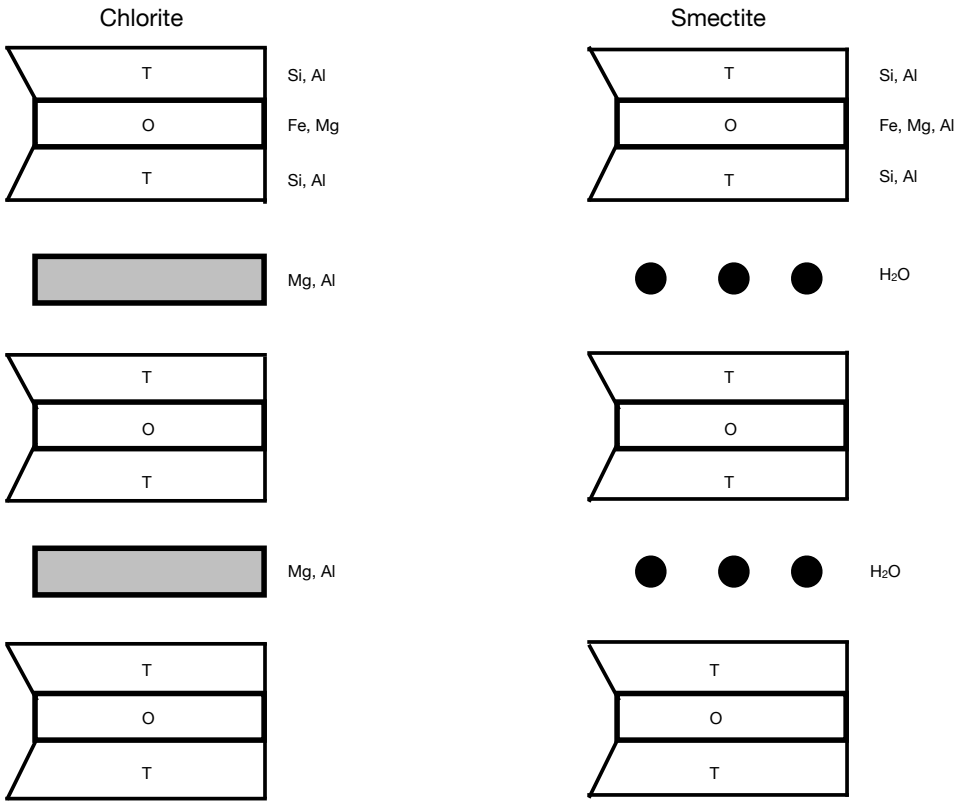

Figure 4: Structural differences between chlorite and smectite clays (modified from Shau et al., 1990).

Corrensite is a smectite-chlorite interlayered clay that may occur either alone or in layers mixed with chlorite (Figure 5) (Beaufort et al., 1997; Brigatti et al., 2013). Corrensite forms in low-temperature conditions during diagenesis or fault movement, usually around 100-200^{o}C and 5-6 km in depth (Murakami et al., 1999; Schleicher, 2012). The dominant mechanism for corrensite crystallization is low-temperature dissolution and precipitation of mafic minerals in the presence of circulating hydrothermal fluids (Beaufort et al., 1997; Murakami et al., 1999; Schleicher et al., 2015). Within rocks of the Franciscan Assemblage in Northern

California, dissolution and precipitation reactions of chrysotile and chlorite minerals form corrensite and other saponitic clays at depth (Schroeder, 2010; Schleicher, 2012). At the SAFOD borehole in Parkfield, California, the gouge contains from 60-100% saponite clay in the surrounding deformation zones (Carpenter et al., 2012).

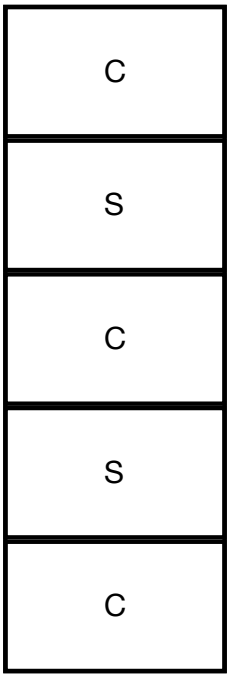

Figure 5: Corrensite is made of smectite (S) and chlorite (C) interlayers (modified from Shau et al., 1990).

Formation

The low-temperature, high-pressure environment within a fault gouge, along with the circulation of water, causes mineral alteration in the upper crust (Moore and Rymer, 2007; Moore, 2014). Laboratory experiments demonstrate that one such mechanism of alteration involves the juxtaposition of ultramafic minerals such as serpentine, with quartzofeldspathic rocks within a fault gouge generating a chemical pathway that drives crystallization of magnesium-rich phyllosilicates (Moore and Rymer, 2012). Magnesium-rich clays such as saponite, corrensite, and talc are formed by the following reaction (Moore and Rymer, 2007; Moore and Rymer, 2012; Moore and Lockner, 2013):

$$Mg_3Si_2O_5(OH)_4 + 2SiO_2 \longrightarrow Mg_3Si_4O_{10}(OH)_2 + H_2O$$

Serpentine + Quartz ⟶ Saponite clay + Water

The section of the San Andreas Fault between the Cholame Valley and San Juan Bautista has the highest creep rates along the transform boundary, up to 28 mm/yr (Moore and Rymer, 2012). SAFOD is located in a portion of this aseismic section, drilled directly into the San Andreas Fault at a depth of 2-3 km. A large serpentinite body exists along the fault boundary at SAFOD and is approximately 2 km thick, running along the transform boundary for 50-60 km (Moore and Rymer, 2007; Moore and Rymer, 2012). XRD analysis of samples from the deformation zone shows that serpentine minerals are being replaced by magnesium-rich clays, such as saponite and corrensite, indicating that chemical reactions are causing the migration of Mg^{2+} ions (Schleicher et al., 2012; Moore,

2014). The change in the chemical composition across the fault results in a chemical potential gradient between the ultramafic-rich lenses and quartzofeldspathic wall rocks, driving a metasomatic exchange across the fault (Moore, 2014). The phyllosilicates alter, with increasing depth, from saponite to corrensite and chlorite (Moore, 2014) (Figure 6).

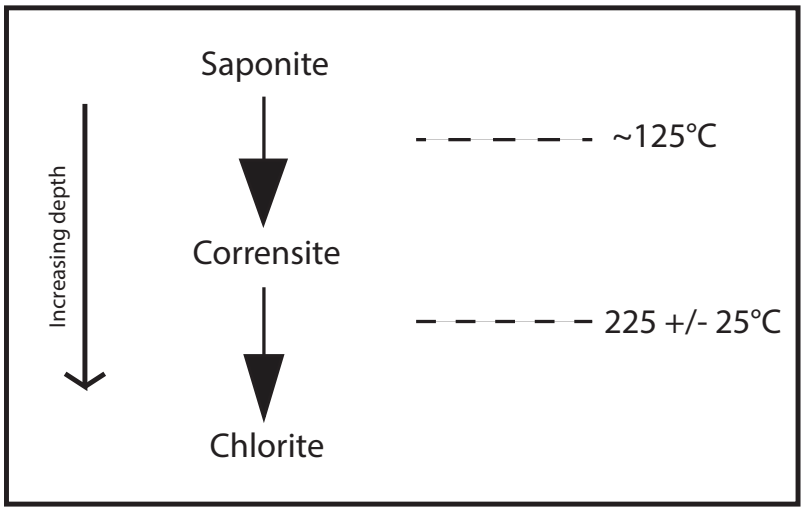

Figure 6: Stability range of magnesium clays at SAFOD (modified from Moore, 2014).

Also at SAFOD, Holdsworth et al. (2010) studied fault gouges where serpentinite is crosscut with calcite veins. In these regions, the gouge matrix is dominated by smectite clays, with clays consisting of over 50% of the total rock volume. Thin section analysis shows multiple generations of recrystallization within the gouge, as evidenced by the brecciation of individual grains and presence of fibrous overgrowths (Holdsworth et al., 2010). Smectite clays are the dominant matrix minerals in creeping faults and have been shown to reduce the coefficient of friction of the gouge to as low as 0.2 (Holdsworth et al., 2010;

Haines and van der Pluijm, 2012). At SAFOD, some of the fault gouges contain more than 60% saponite clay, while some of the smaller shear zones at SAFOD may contain up to 100% saponite clay (Carpenter et al., 2012).

In a similar study, Schleicher et al. (2010) noted that “nanocoatings” of illite-smectite and chlorite-smectite clays form on the core drilled in SAFOD. These clays crystallized under low temperature conditions near the surface. Dissolution of serpentine minerals or chlorite within the fault line results in a magnesium-rich fluid which crystallizes smectite clays (Schleicher et al., 2010). Their crystallization indicates that interlayered clays, such as corrensite, may grow within the gouge during creep in the shallow crust at very low temperatures (Schleicher et al., 2010; Haines and van der Pluijm, 2012). Haines and van der Pluijm (2012) and Schleicher et al. (2015) noted similar mineralogical environments in low-angle normal faults of the western United States and on the Alpine Fault in New Zealand where low-temperature solution transfer reactions cause the formation of various smectite clays due to fluid circulation within the gouge.

Mechanical Properties

Magnesium-rich phyllosilicates have distinctive frictional properties (Moore and Lockner, 2007; Haines and van der Pluijm, 2012; Tesei et al., 2012; Schleicher et al., 2015). For these platy minerals, frictional strength has a direct relationship with bond strength between the layers. The bond strength has, in turn, an inverse relationship with the thickness of a film of water that maintains these bonds. The thicker the film of water between platy layers, the weaker the bonds are between those layers (Moore and Lockner, 2007; Tesei et al., 2012).

Fault gouges containing a high proportion of trioctahedral expanding clays have significantly different mechanical properties than those without (Moore and Rymer, 2012; Tesei et al., 2012; Schleicher et al., 2015). Saponite, corrensite, and talc all exhibit stable sliding behavior under high shear stress. This stable sliding behavior results in a continual shear at constant velocity, the same movement that characterizes aseismic behavior of a fault (Moore and Rymer, 2007; Moore and Lockner, 2013; Janssen et al., 2014).

Additionally, the high pore pressure of trioctahedral expanding clays can significantly lower the coefficient of friction along a fault plane (Tesei et al., 2012). Water contained between the clay layers increases the pore pressure within a fault gouge. By increasing the pore pressure within a fault gouge, the coefficient of friction is decreased, causing movement along a fault line (Tesei et al., 2012). Because corrensite is a 2:1 layer clay that contains water between tetrahedral

layers, it has a high pore pressure, lowering the frictional strength of faults (Tesei et al., 2012; Schleicher et al., 2015).

Tesei et al. (2012) studied the relationship between magnesium phyllosilicate crystallization and fault movement along low-angle normal faults in central Italy. Within the seismogenic zone in this region, chlorite and serpentine minerals recrystallize into illite and chlorite-smectite clays, including corrensite. Tesei et al. (2012) used both powdered and solid-rock samples of magnesium-rich clays under biaxial deformation to determine the relationship between phyllosilicate content and the coefficient of friction. Phyllosilicate content of the various samples ranged from 0 to 52 weight % and experiments were run under dry conditions at constant normal stresses of both 20 and 50 mPa (Tesei et al., 2012). Results of Tesei et al.'s experiments (2012) indicate that the deformation of individual grains in these samples is accommodated by frictional and grain-to-grain sliding, as the (001) planes of the phyllosilicates create multiple weak planes within the gouge, resulting in stable sliding behavior (Tesei et al., 2012). Fault gouges containing as little as 20% phyllosilicates can alter the coefficient of friction from 0.6 to 0.4. The more phyllosilicate-rich a gouge is, the lower the coefficient of friction. The effect of phyllosilicate content on friction can be even further enhanced with water movement, especially in an environment containing serpentine minerals or chlorite (Tesei et al., 2012; Moore, 2014).

The lower coefficient of friction, combined with stable sliding behavior, produces creep along a fault (Moore and Rymer, 2007, 2012; Tesei et al., 2012; Moore 2014; Schleicher et al., 2012, 2015). Studies done at the bore hole at SAFOD and along the Alpine Fault in New Zealand mirror these results (Schleicher, 2010; Carpenter, 2012; Schleicher et al., 2015).

STUDY AREA

Sampling Locations

In order to test the hypothesis that faults to the northeast of LLV are creeping, samples were collected from three fault gouges northeast of LLV and tested for magnesium-rich phyllosilicate content (Figure 7). Two of the sampling locations were previously studied by Schroeder (2010), and one additional site was included. Samples collected at Sites #1 and #2 are fault gouges within the MFZ that were identified by Schroeder (2010) as Locations 10 and 11. In addition, Site #3 for this study was identified along a previously-unmapped fault within a streambed (Figure 7).

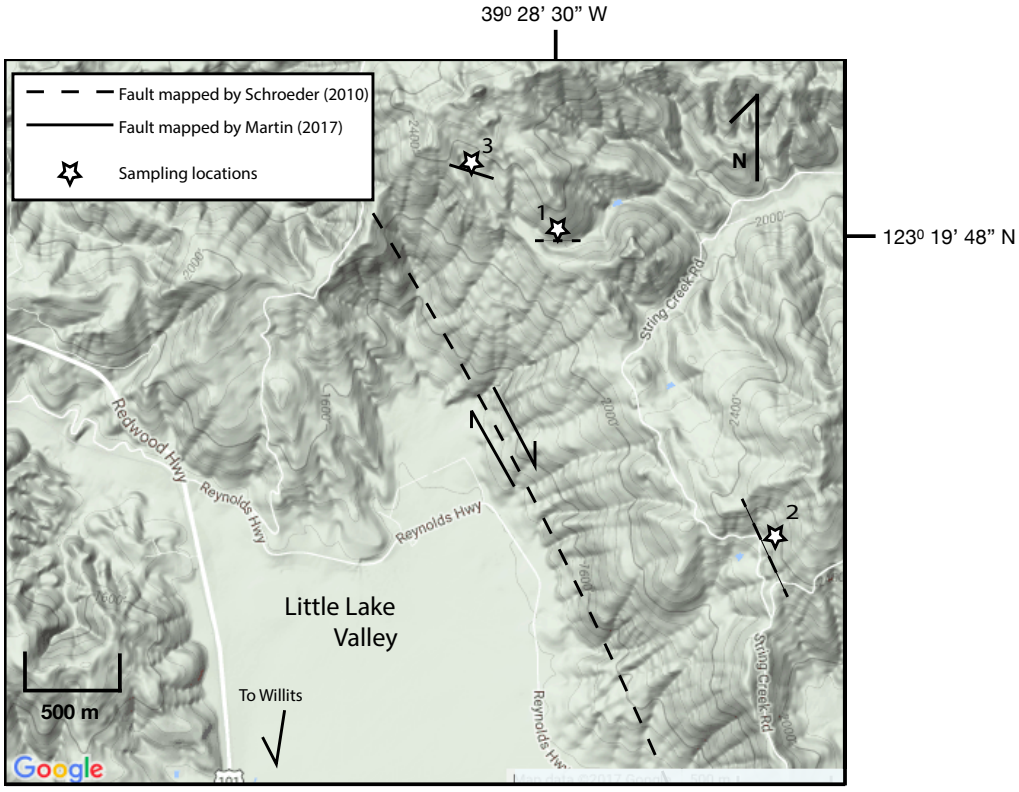

Figure 7: The three sampling locations described in this paper.

Site #1

Site #1 was identified as Location 10 by Schroeder (2010). He described this location as intermingled greywacke and meta-volcanic rocks within a serpentinized fault gouge (Figure 8). This site was accessed through private property along String Creek Road in Mendocino County (39 deg, 28 min, 30 sec N; 123 deg, 19 min 48 sec W; Zone 10S, 4369542 N, 471617 E). The site sits at 670 m in elevation within the creek bed of a seasonal stream named the Middle Fork of String Creek. The sampling location is about 1 km upstream from where the middle fork joins the main String Creek channel.

The outcrop is a fault gouge developed within bedrock, about 1.8 m deep and 2 m wide (Figure 8). The bedrock is a melange unit of Central Belt Franciscan Assemblage that has been exposed by the erosional action of the seasonal stream (Figure 8). The gouge runs through the plane of the creek bed, from one side to the other, along a west-east strike, coinciding with a 90◦ turn in the streambed. Schroeder (2010) called this location a “fish-hooked” stream. Samples were taken in a transect from the competent rock on the northern side, through the fault gouge, and into the competent rock on the southern side. The rock within the gouge is heavily weathered with large veins of white calcite extending deep into the gouge.

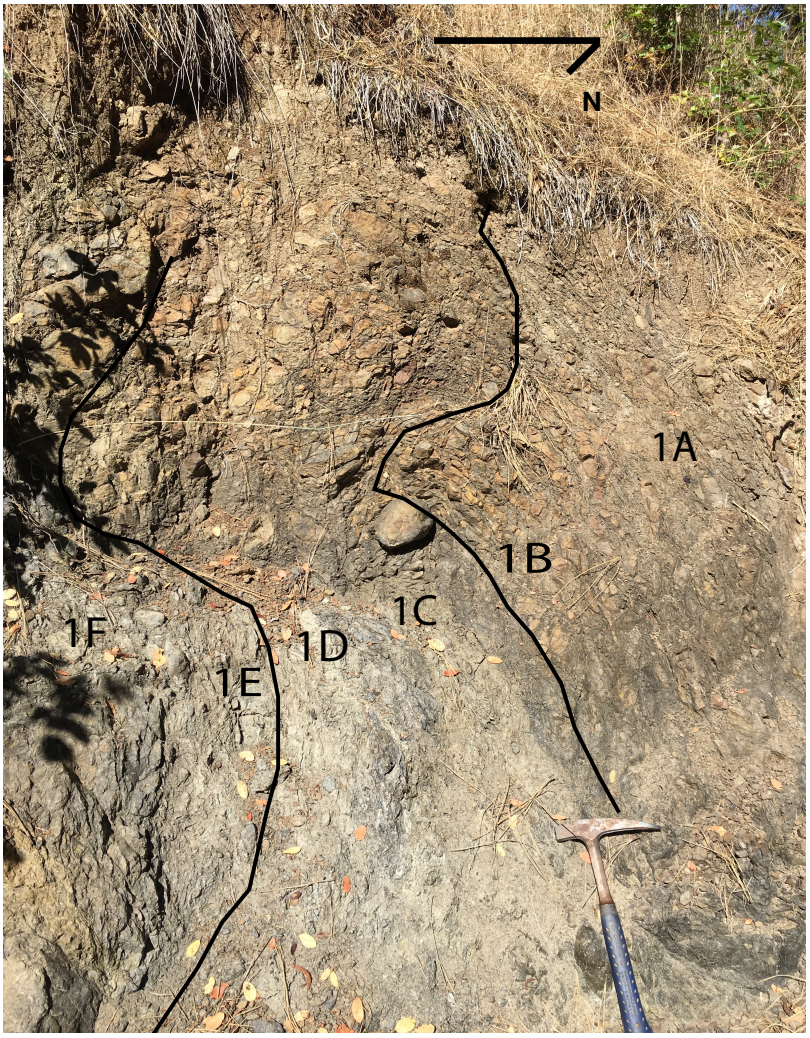

Figure 8: Site #1 showing the outline of the fault gouge along the MFZ. Samples 1A-1F were collected in a north-south transect across the gouge.

Sample 1A was taken from competent meta-greywacke, just to the north of the main fault gouge. This meta-greywacke becomes more fractured as the gouge boundary is approached. The rock is very dark green to black with some calcite veining. Petrographic analysis shows that the rock consists of a very fine groundmass that becomes more foliated toward the fault gouge. The groundmass consists of quartz and albite grains, becoming increasingly foliated

with increasing magnesium-phyllosilicate content. Veins of calcite cut through most of the rock.

Sample 1F was taken from the consolidated rock south of the main fault gouge. The rock on this side of the gouge is blueschist. These rocks are heavily iron-stained. Samples 1B through 1E were taken in a transect across the fault gouge, from north to south (Figure 8). Petrographic analysis shows decreasing amounts of meta-greywacke towards the north of the gouge, grading into fragmental blueschist toward the south. Material within the gouge is highly unconsolidated with calcite veining and iron stains due to weathering and water movement along the gouge.

Samples were also taken from the bedrock on the east side of the creek bed. This portion of the outcrop did not show the fault gouge, although the rock was highly sheared. Samples 1K and 1L were taken from this portion of the outcrop, which is approximately 1 m by 1 m in size (Figure 9). These wall rocks consist of a phyllosilicate-rich greywacke, which becomes more foliated towards the fault.

Figure 9: Opposite side of the creek bed from Site #1. Samples 1K and 1L were taken here.

Site #2

Site #2 was identified by Schroeder (2010) as Location 11. He described this location as a highly sheared, serpentinized fault gouge with evidence of a recent landslide nearby (Schroeder, 2010). This outcrop is located in a roadcut along String Creek Road at 695 m in elevation (39 deg, 27 min, 42 sec N, 123 deg 19 min, 3 sec W; 4368050 N, 472665 E). The full outcrop is 4.5 m high and 3.5 m wide and is located within a large hole dug into the hillside along String Creek Road (Figure 10). This cut revealed a north-south striking fault (355 degrees) with a nearly vertical dip running through the right-hand side of the outcrop. The

gouge consists of highly sheared greywacke and more chlorite-rich greywacke, running along two distinct planes. Between these fault planes rests a large block of competent greywacke. This block deflects the fault plane, which encircles it in two directions to continue its propagation.

A competent block of greywacke lies to the north of the fault gouge. It is well consolidated and dark green to black. The fault gouge consists of sheared greywacke towards the west, then becomes a lighter tan closer to the gouge. The eastern side of the outcrop has a similar block of dark green to black greywacke. The easternmost portion of the fault gouge is occluded by alluvium.

Figure 10: Site #2 with north-south trending fault cutting through greywacke.

Site #3

Site #3 is a fault within a creek bed to the west of Site #1 at 668 m in elevation (39 deg, 28 min, 33 sec N; 123 deg, 19 min, 55 sec W; 43696444N, 471444 E). This fault strikes at 115 degrees and dips 35 degrees southwest (Figure 11). This orientation roughly correlates with the fault at Site #1, which strikes approximately E-W. Although Site #1 and Site #3 are only separated by 300-400 m, the two streams drain separate watersheds. Site #1 sits in the Middle Fork of String Creek, draining into String Creek towards the east, and eventually into the Russian River drainage to the south of Willits. The seasonal creek containing Site #3 is unnamed and drains directly south into LLV, eventually draining north into the Eel River drainage system, north of Willits. There is an abrupt change of slope about 20 m downstream of the fault gouge where the stream becomes a waterfall into LLV.

Site #3 contains highly weathered and chlorite-rich greywacke on both sides of the fault gouge (Figure 11). The greywacke is highly foliated and fractured, with foliation increasing towards the actual gouge. Calcite veining is in both the fault gouge and in the massive meta-greywacke deposits on the ridges to either side of the fault. A vein of tremolite runs along the fault plane within the fault gouge. This light green tremolite is very soft and is mixed with chlorite. Handfuls of tremolite can be easily scooped out of the vein.

Figure 11: Sheared meta-greywacke within the fault gouge at Site #3. Note the light green tremolite vein cutting along the fault plane.

ANALYTICAL METHODS

A total of twenty-one samples were taken from the three fault gouge study sites. In order to do petrographic analysis, thin sections were made of all the samples collected from Sites #1 and #2. However, thin sections were only made for a subset of samples from Site #3 because several samples were too soft to prepare thin sections. Following petrographic analysis, samples from all three sites were powdered for XRD analysis at the U.S. Geological Survey in Menlo Park, California using a Rikagu Multiflex x-ray diffractometer. X-rays were generated by copper Kα radiation and run at 40 kV and 20 mA. Scan range was 2 to 70 degrees at 2°/minute and 0.010-degree sampling width. Samples containing a high percentage of magnesium-rich clay minerals were glycolated over two days and re-tested. Glycolating causes the layered clays to expand and shifts the positions of the mineral peaks due to expansion of the clay mineral structure, aiding in identification (Tesei et al., 2012; Moore, 2014).

After XRD analysis, samples with a high proportion of magnesium clays were viewed through a scanning electron microscope at the U.S. Geological Survey in Menlo Park using a Tescan VEGA3 Variable W-filament Scanning Electron Microscope (SEM) equipped with Energy Dispersive Spectroscopy (EDS). The EDS is an Xmax 50 SDD.

RESULTS

Site #1

Petrographic analysis revealed that the fault gouge at Site #1 is meta-greywacke in contact with blueschist. Chert was also discovered at this gouge, which is a common rock in Franciscan melange material (Woolace, 2005; Schroeder, 2010). Figure 12 is a photomicrograph of Sample 1A, which was taken from competent meta-greywacke wall rocks to the north of the gouge at Site #1. This sample consists of fine-grained, equigranular meta-greywacke with veins of calcite running along fractures in the rock. Chlorite also exists in this sample, as determined by XRD analysis.

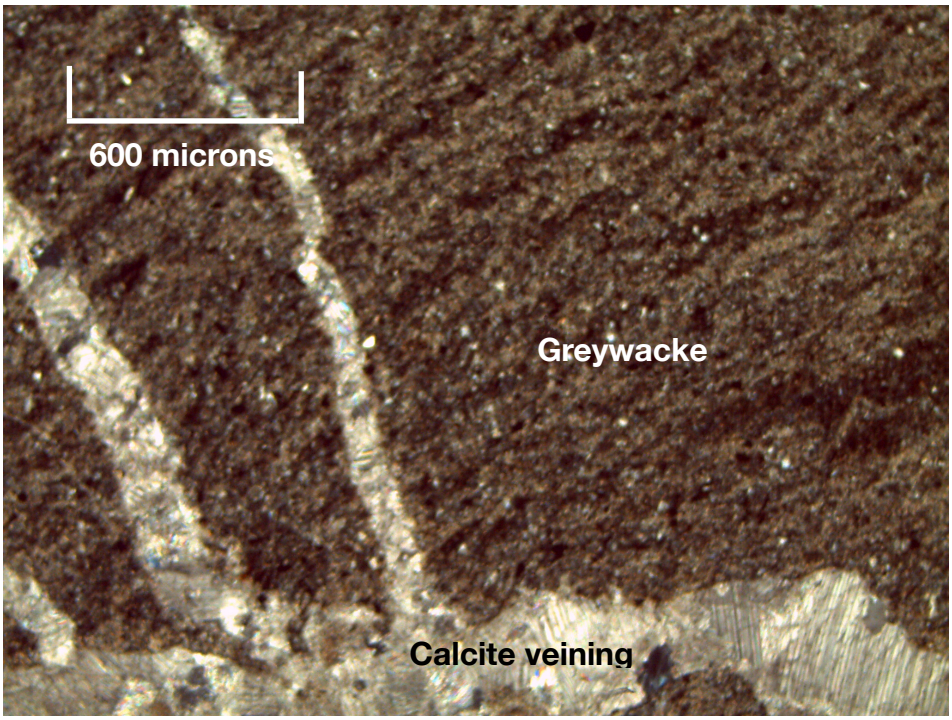

Figure 12: Sample 1A under cross-polarized light. Massive meta-greywacke is cut by veins of calcite.

Figure 13 is a photomicrograph of Sample 1J taken from the wall rocks which lie to the south of the fault gouge at Site #1. Sample 1J is a fine-grained, foliated blueschist-facies rock with abundant glaucophane, or other Na-rich amphibole, and albite.

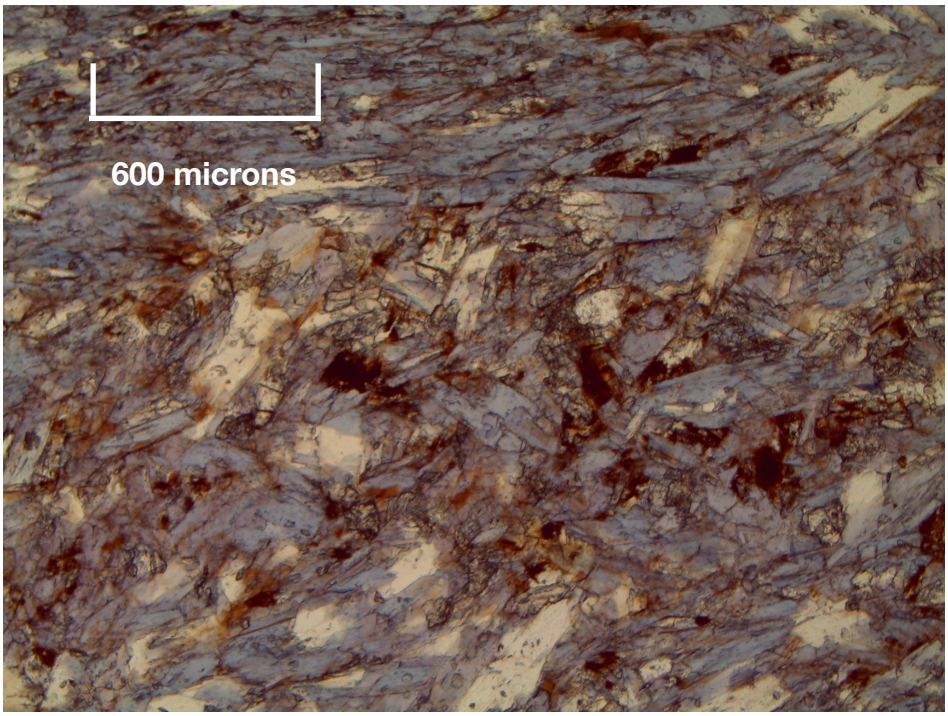

Figure 13: Blueschist in Sample 1J under plane-polarized light. Note the abundant blue glaucophane.

Figures 14 and 15 are photomicrographs of sample locations 1C and 1D. Both of these samples were taken within the fault gouge and contain the expanding, magnesium-rich clay corrensite, as determined by XRD. Both samples had fabrics typical of active deformation, including aligned clay minerals with weak foliation (Janssen et al., 2014). XRD and SEM data indicated a high proportion of calcite in both samples. Both foliation and calcite content increased from the wall rocks into the center of the fault gouge.

Highly brecciated quartz and feldspar grains show extensive fractures (Figure 15). A slight foliation developed along fractures between the grains, which contains abundant iron oxides and calcite. Clay minerals within veins contain the highest proportion of corrensite.

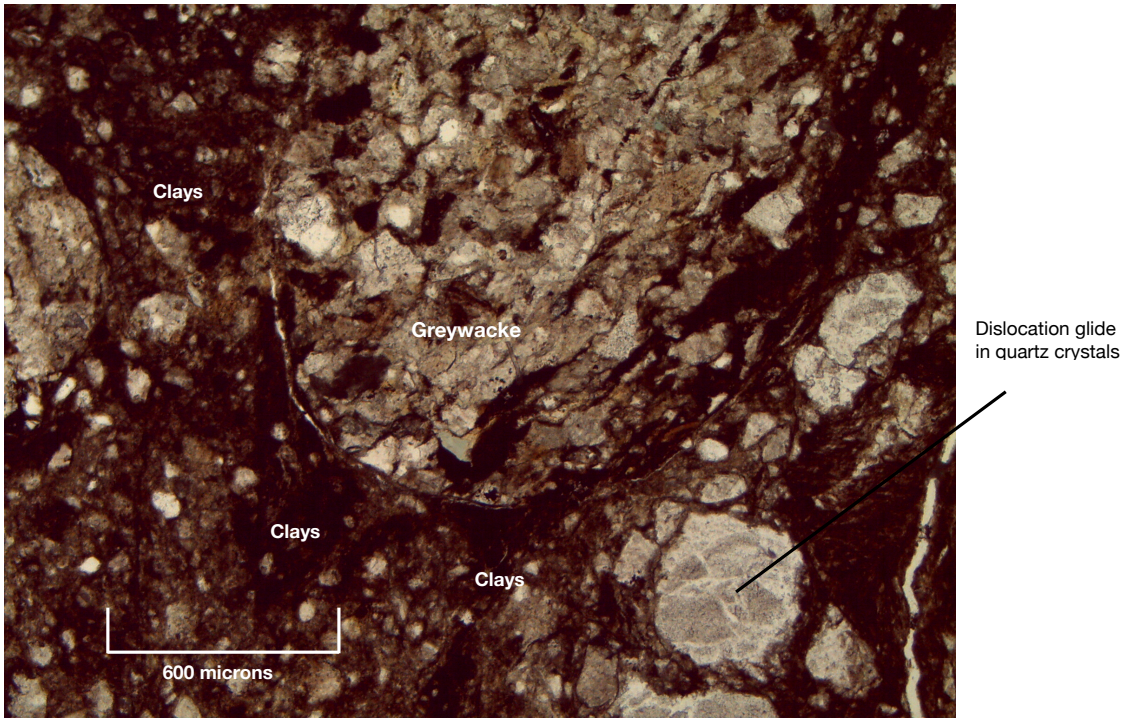

Figure 14: Photomicrograph of sample 1C, from the fault gouge at Site #1 under plane polarized light. Quartz and feldspar within large grains of meta-greywacke show evidence of cataclasis. Clay minerals occur along the boundaries between grains.

Sample 1D (Figure 15) is very similar to Sample 1C and contained fractured meta-greywacke with abundant phyllosilicates. Corrensite has crystallized by pressure-solution recrystallization within veins between the large meta-greywacke grains. This sample also contained more calcite within a very fine quartz/feldspar groundmass.

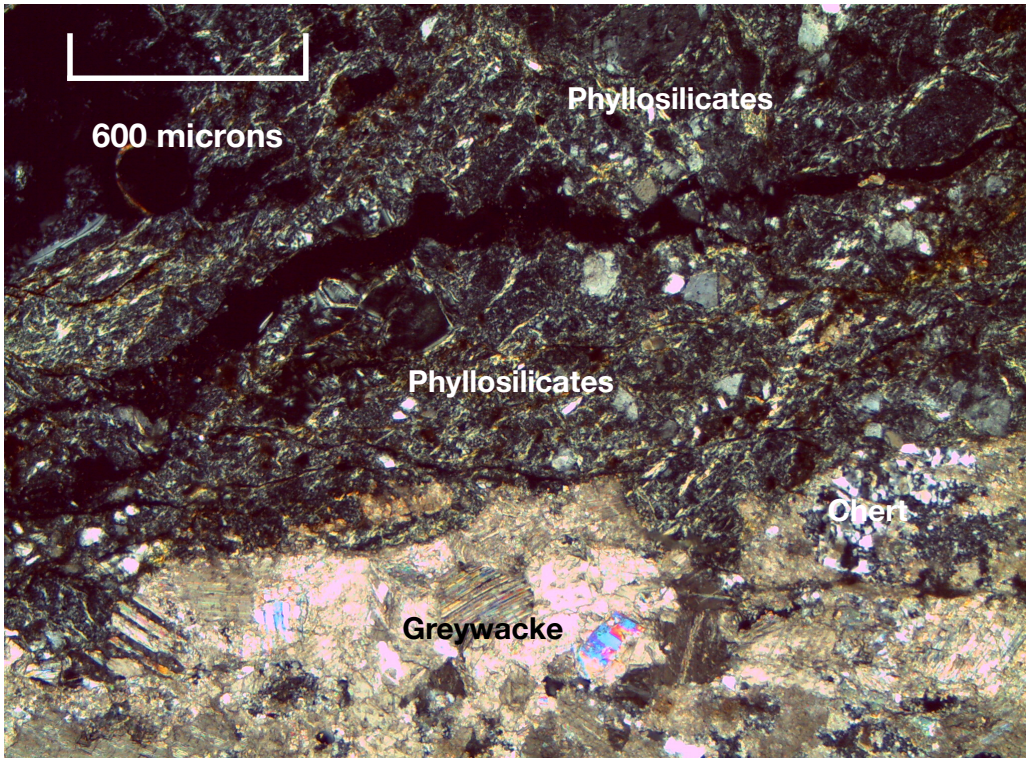

Figure 15: Photomicrograph of sample 1D, from the fault gouge at Site #1, under cross polarized light. Clay minerals are deposited along the contacts between quartz and feldspar grains within the greywacke. Chert can be seen in the right side of the photo, just below the phyllosilicates. The highly birefringent mineral grains are white micas, which are found throughout the fractured greywacke.

Meta-greywacke from both the wall rocks and the gouge at site #1 contains some large chlorite crystals, but chlorite is also found within the quartz-feldspar groundmass. Other magnesium-rich phyllosilicates fill the veins. XRD analysis indicates that samples from both Sites #1 and #2 contain chlorite, which is common as a secondary mineral in rocks of the Central Belt Franciscan Assemblage (Woolace, 2005; Schroeder, 2010). Based on XRD results, corrensite is abundant in the fault gouge at Site #1, but is absent from the meta-

greywacke wall rocks on the north side of the gouge and in the blueschist wall rocks on the southern side of the fault gouge.

Figures 16-19 show XRD patterns of the samples containing magnesium-rich clays in samples 1C and 1D. Both samples were taken from the center of the gouge at Site #1 (Schroeder's Location 10). Untreated samples of 1C and 1D were x-rayed, then glycolated and left overnight. The corrensite peak was identified from the powder diffraction patterns by the double peak at 12.5° 2θ and a d-spacing of 7.0-7.5. Glycolation caused the single peak at 12.5° to shift into a double-peak of the interlayer clays corrensite+chlorite (Moore personal communication, 2017). Glycolation also shifts the other corrensite peaks at 19.65-19.76° and 25.13° 2θ. However, chlorite peaks remain stable, as chlorite does not contain water within the interlayers. Additionally, these samples show strong chlorite peaks at ~ 5.8° and ~ 13°.

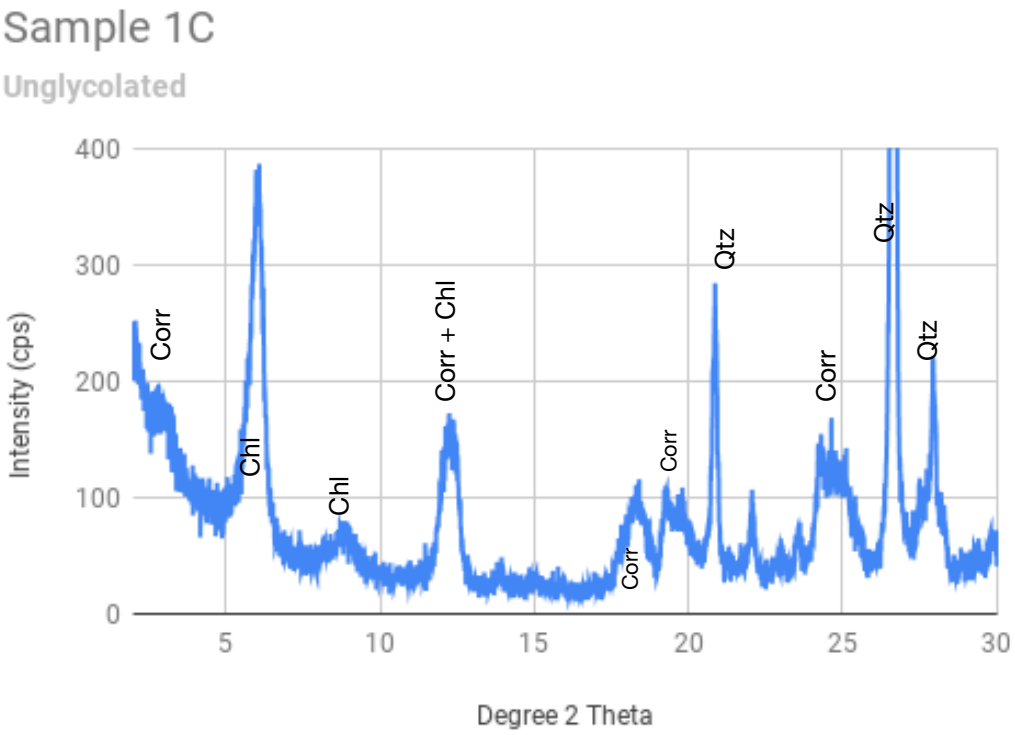

Figure 16: Rock powder x-ray diffraction patterns for untreated sample 1C taken from the fault gouge at Site #1. Peaks for quartz (Qtz), chlorite (Chl), corrensite (Corr), and corrensite + chlorite (Corr + Chl) all noted.

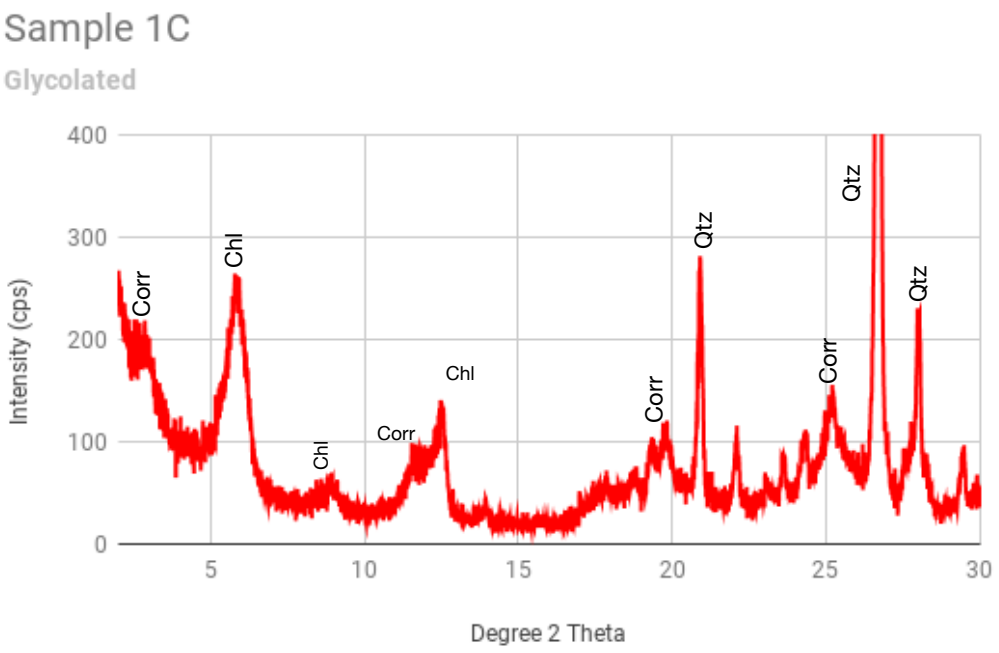

Figure 17: Rock powder x-ray diffraction patterns for glycolated sample 1C taken from the gouge at Site #1. Peaks for quartz (Qtz), chlorite (Chl), and corrensite (Corr) all noted.

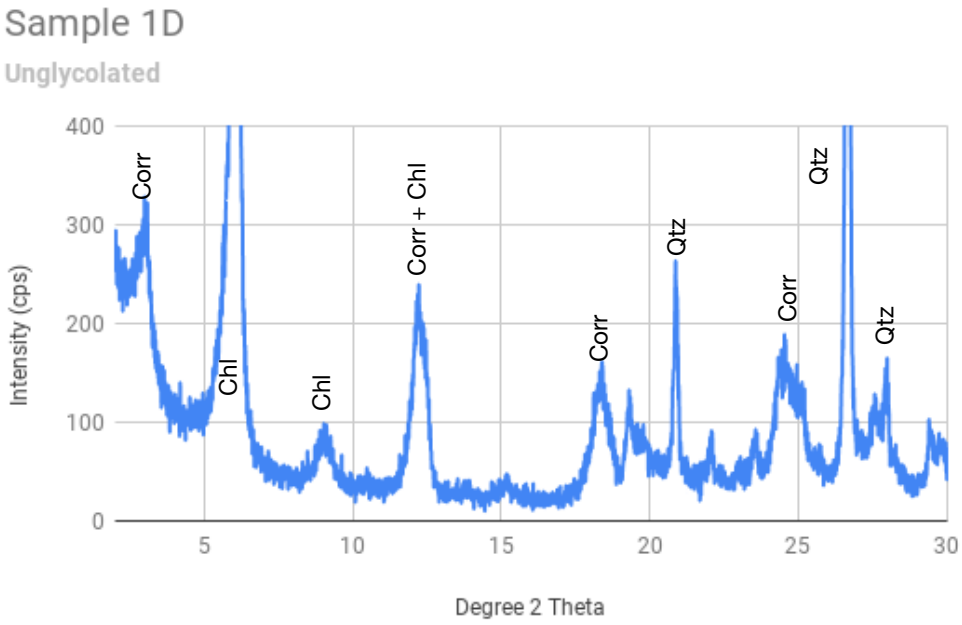

Figure 18: Rock powder x-ray diffraction patterns for untreated sample 1D taken from the gouge at Site #1. Peaks for quartz (Qtz), chlorite (Chl), corrensite (Corr), and corrensite + chlorite (Corr + Chl) all noted.

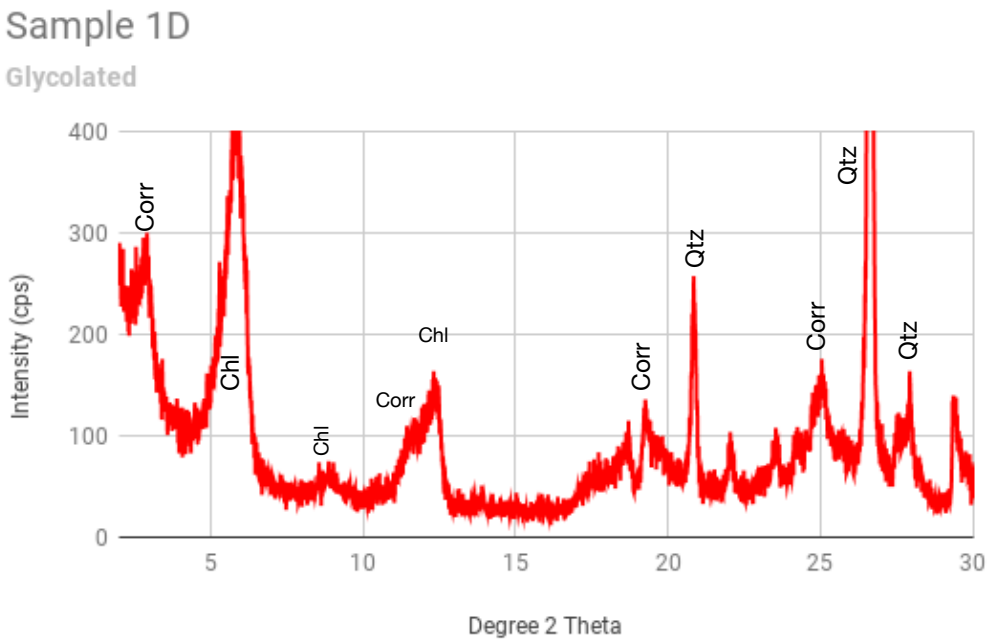

Figure 19: Rock powder x-ray diffraction patterns for glycolated sample 1D taken from the gouge at Site #1. Peaks for quartz (Qtz), chlorite (Chl), and corrensite (Corr) all noted.

The SEM was used to document the relationship of the magnesium-rich phyllosilicates to the surrounding mineral grains, and energy dispersive spectroscopy (EDS) was used to obtain qualitative analyses of the minerals present. Figure 20(a) is a photomicrograph of Sample 1C showing brittle deformation of quartz and feldspar grains within the meta-greywacke groundmass. Chlorite grains show evidence of cataclastic flow within the rock, which commonly occurs in melange units with high water content (Cowan, 1978; Schleicher et al., 2015). EDS results for corrensite are shown in Figure 20(b).

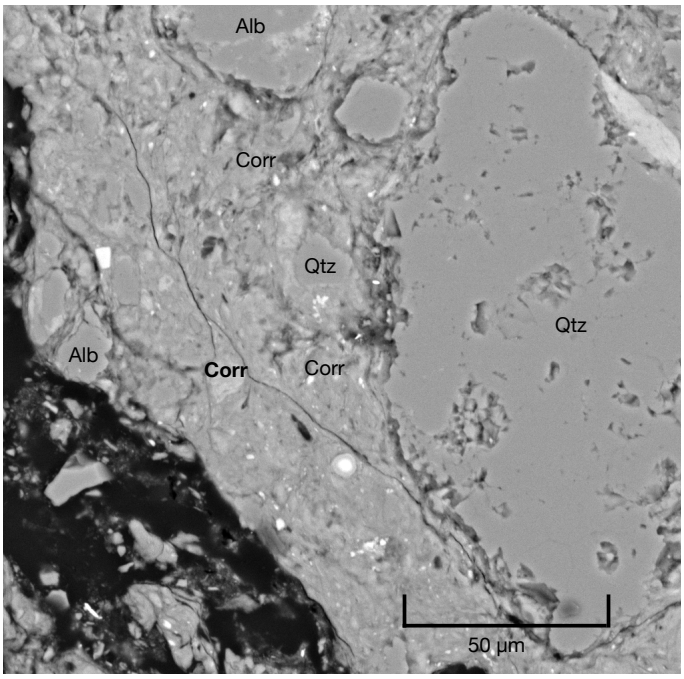

(a)

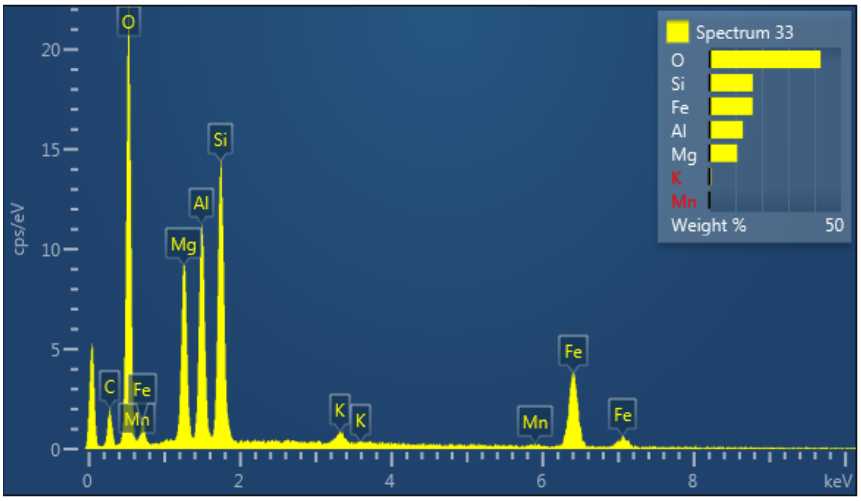

(b)

Figures 20 (a) and (b): SEM photomicrograph of Sample 1C with representative EDS spectra for corrensite. Large quartz (Qtz) and albite feldspar (Alb) grains have undergone brittle deformation. The large corrensite (Corr) crystals are alteration products, while more phyllosilicates fill the veins. Cataclastic flow has occurred between the large grains. (b) EDS analysis for corrensite grain in bold type.

Figure 21(a) is a photomicrograph of Sample 1D showing the relationship of the clays to surrounding minerals within the gouge. The sample has evidence of cataclastic flow within the gouge as quartzofeldspathic minerals are broken by brittle deformation in the veins. Again, the larger grains of chlorite exist within the quartzofeldspathic groundmass while fine-grained corrensite recrystallized in veins. Figures 21 (b-d) show EDS results for corrensite grains identified on Sample 1D.

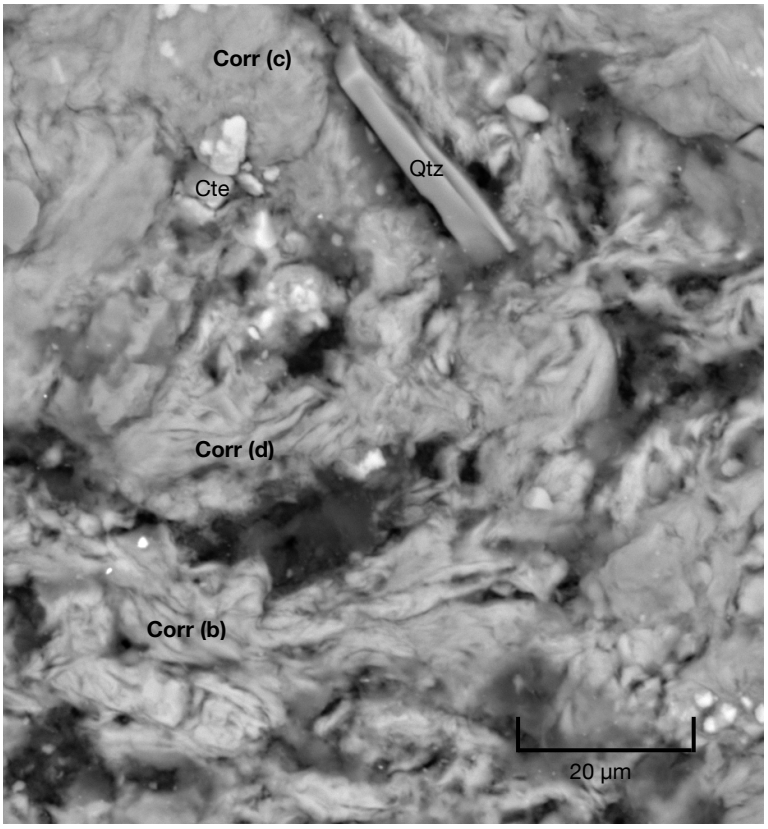

(a)

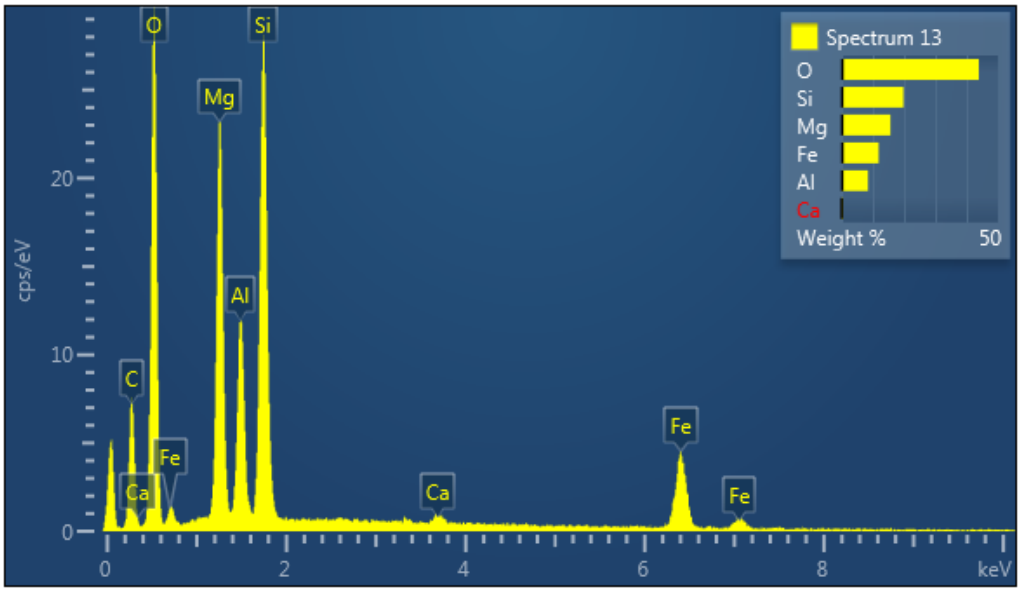
Spectrum 13
O
Si
Mg
Fe
Al
Ca
Weight %
50
cps/eV
20
10
0
O
Si
Mg
Al
C
Fe
Ca
Ca
Fe
Fe
0
2
4
6
8
keV

(b)

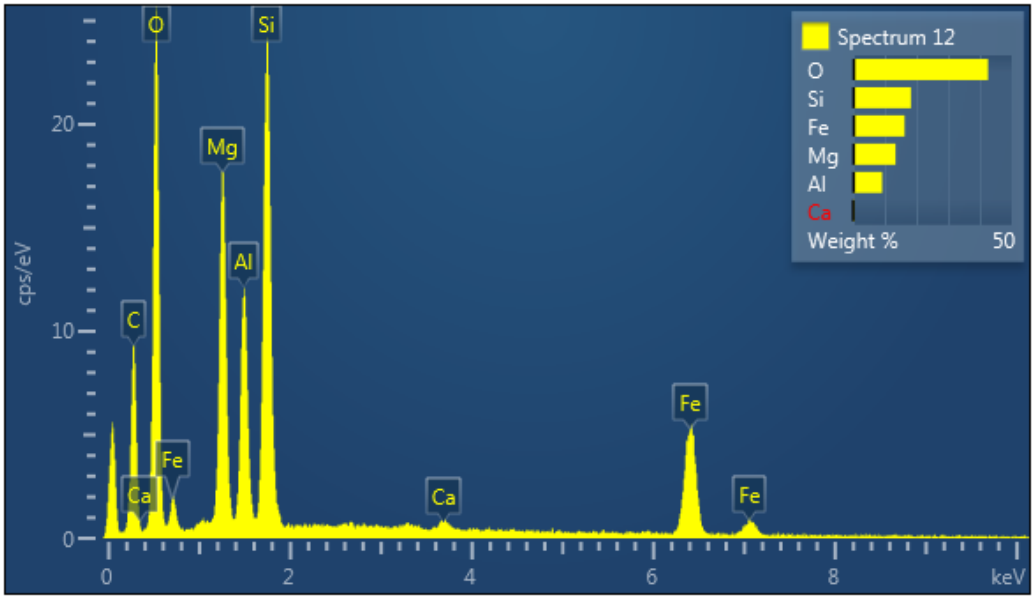
Spectrum 12
O
Si
Fe
Mg
Al
Ca
Weight %
50
cps/eV
20
10
0
O
Si
Mg
Al
C
Fe
Ca
Ca
Fe
Fe
0
2
4
6
8
keV

(c)

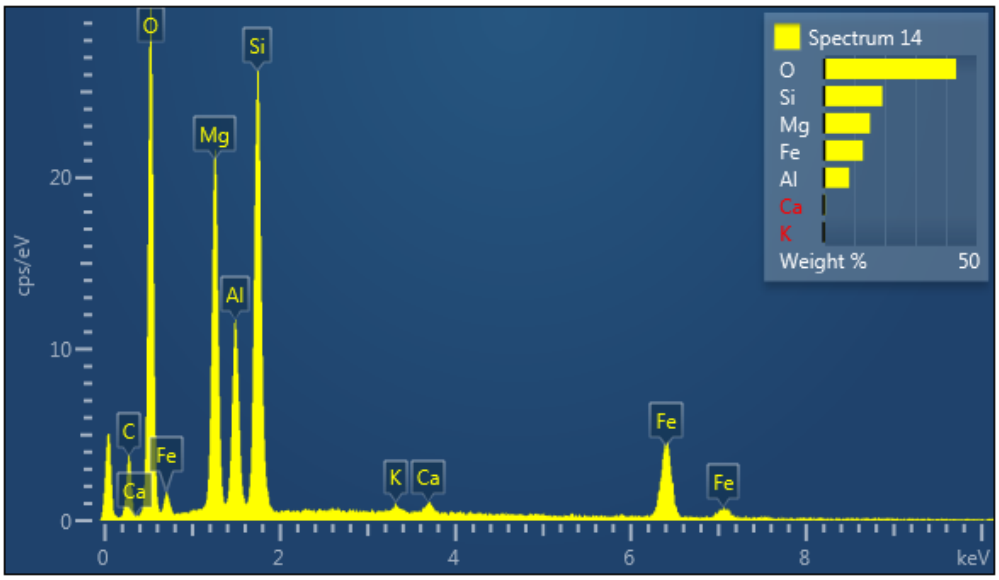

(d)

Figure 21 (a-d): Photomicrograph of corrensite (Corr) in Sample 1D at Site #1. The corrensite is mixed with quartz (Qtz), and calcite (Cte). Corrensite is formed in the veins, indicating evidence of water flow along the fault. Figures 21 (b)-(d) show EDS analyses for corrensite grains indicated in bold type in the sample.

Figure 22(a) is also a photomicrograph of Sample 1D showing brittle deformation of quartz crystals surrounded by deposits of chlorite. SEM photos indicate that phyllosilicates make up 30-50% of Samples 1C and 1D. Figures 22(b) and (c) show qualitative analysis of corrensite and chlorite from Figure 22(a), also obtained by EDS.

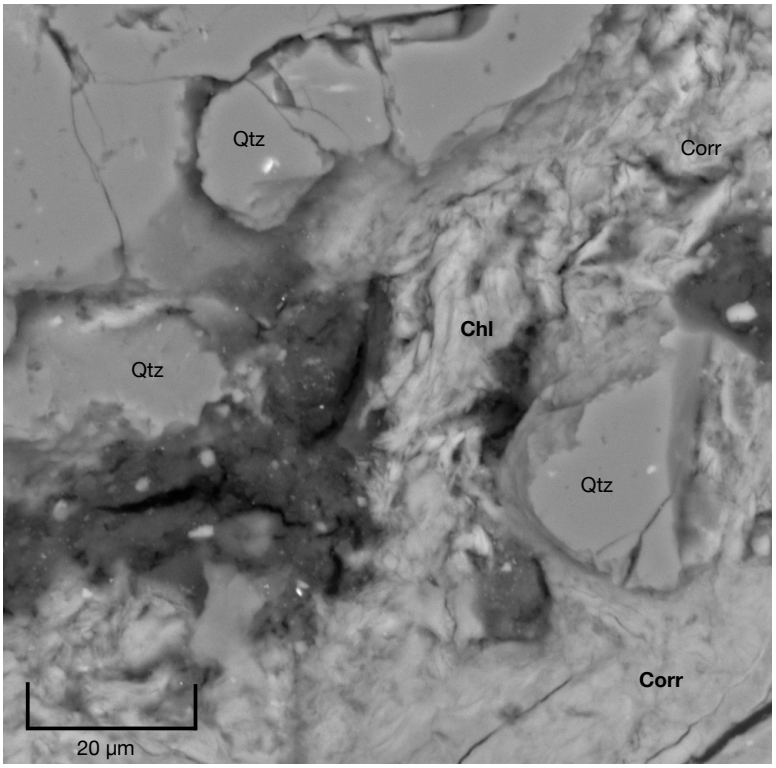

(a)

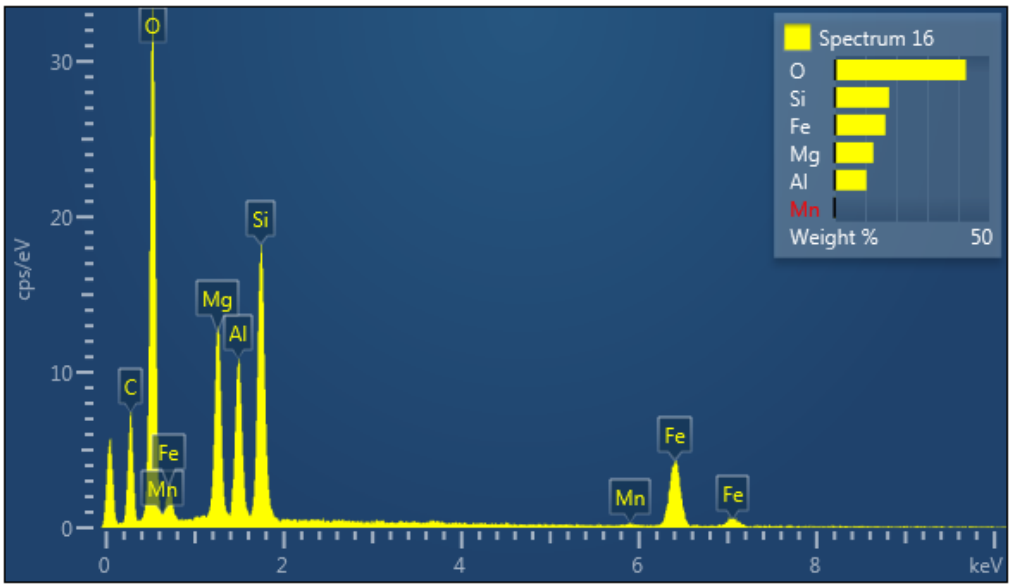

(b)

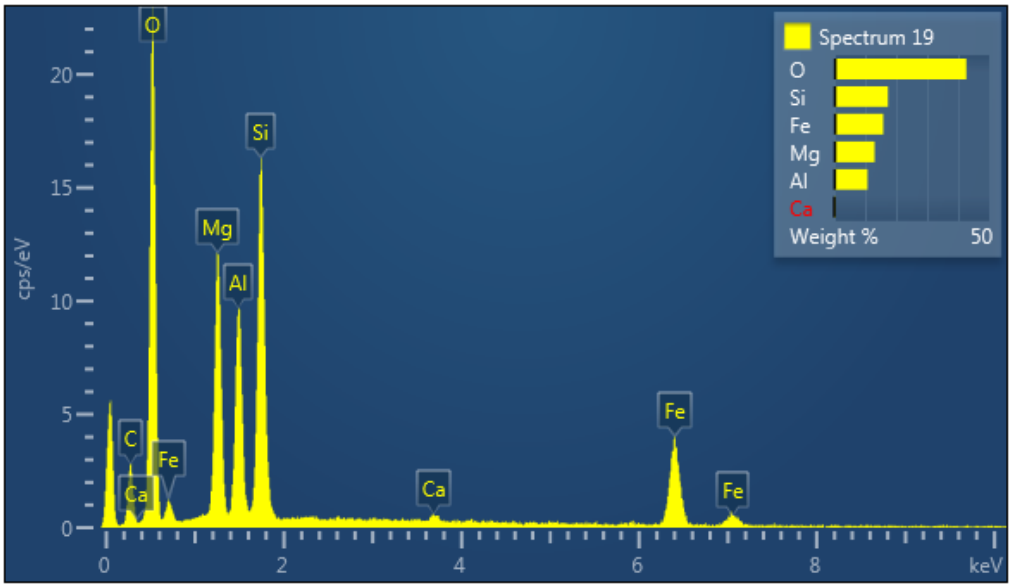

(c)

Figure 22 (a-c): Photomicrograph of chlorite (Chl) and corrensite (Corr) in Sample 1D. Note cataclasis of quartz grains with chlorite deposited within the fractures. Figure 22 (b) shows EDS analysis of chlorite and 22 (c) shows EDS analysis of corrensite in Sample 1D.

Semi-quantitative analyses of corrensite, corrensite+chlorite, and chlorite are shown in Table 2. Cations were calculated on the basis of 25 oxygens for corrensite and 28 oxygens for chlorite (Moore, 2014).

Table 2: Representative compositions of Mg-phyllosilicates from samples 1C and 1D.

	Corrensite	**Corrensite-Chlorite**	**Chlorite**
SiO_2	38.97	42.24	37.81
Al_2O_3	17.28	15.98	19.58
FeO	20.89	15.26	21.26
MnO	0	0	0
MgO	22.23	25.84	20.87
CaO	0.63	0.68	0
K_2O	0	0	0
Total	100	100	99.52
Si	6.098	6.410	6.636
Al (IV)	1.902	1.590	1.364
Al (VI)	1.285	1.268	2.687
K	0	0	0
Ca	0.106	0.111	0
Mn	0	0	0.069
Mg	5.185	5.845	5.461
Fe	2.734	1.937	3.121
O	25	25	28
Si/(Si + Al)	0.657	0.691	0.621
Mg/(Mg + Fe)	0.655	0.751	0.636
Al^{VI} + Mg + Fe	9.204	9.05	11.269
Ca + K	0.106	0.111	0

Note: Weight percents for oxides were normalized to 100. One SEM-EDS spectra was taken as representative for corrensite, corrensite+chlorite, and chlorite.

Sites #2 and #3

Site #2 consists of greywacke in contact with greywacke, with brittle deformation of greywacke within the fault gouge. This location also contained chlorite within the fault gouge; however, no other magnesium-rich phyllosilicates were present. Petrography and XRD analysis indicate that the gouge contains a high proportion of quartz and feldspar with scarce magnesium-rich minerals. Figure 23 shows a photomicrograph of the gouge at Site #2 with highly fractured quartz and feldspar grains within a fine-grained greywacke matrix. Chlorite was evident within the greywacke groundmass, but no fine-grained phyllosilicates were formed within any veins in the rock.

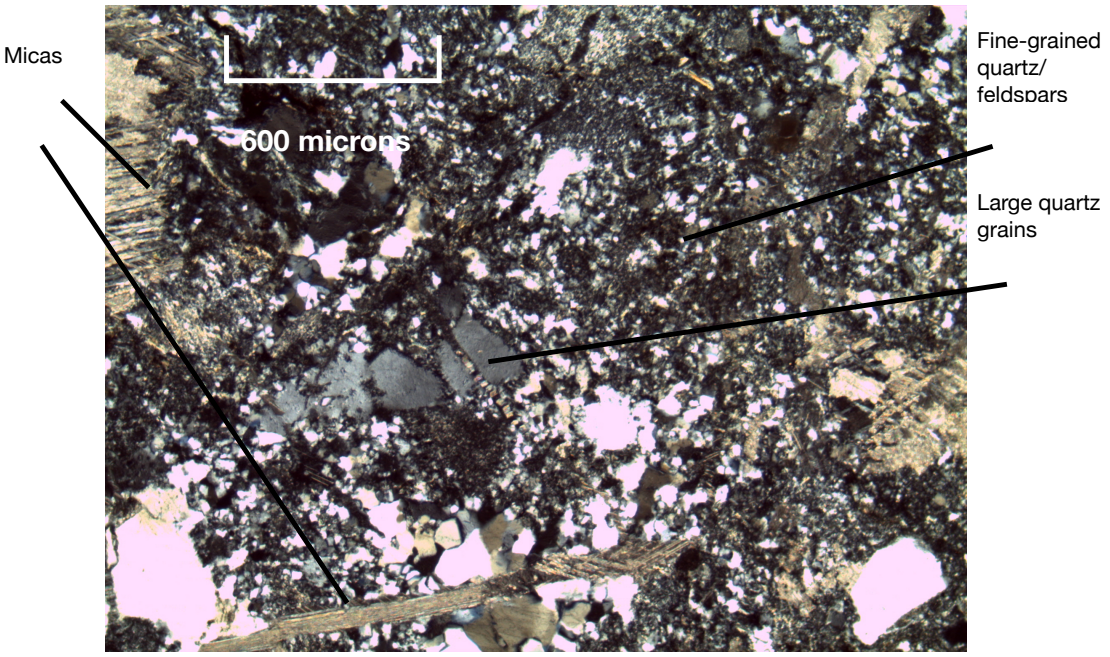

Figure 23: Photomicrograph of gouge at Site #2. Large, fractured quartz and feldspar grains are contained within a fine-grained greywacke matrix. Note the lack of fractures for fluid flow that was indicative of Site #1.

Both sites #2 nor #3 were rich in quartzofeldspathic minerals due to the brecciation of greywacke; however, neither contained any other magnesium-rich clay mineral besides chlorite. Although Schroeder (2010) identified serpentine minerals at Site #2, none were found in this study. XRD analysis indicated a low proportion of magnesium and iron in samples from Sites #2 and #3, reducing the possibility of any serpentine minerals within the gouge (Moore, 2014; Moore, personal communication, 2017).

Additionally, petrographic analysis of samples from Site #3 indicates highly sheared meta-greywacke in contact with meta-greywacke across the fault. The gouge at this particular site is highly foliated along the fault plane. Petrography and XRD analysis shows that samples from this site are meta-graywacke similar in composition to samples from Site #2. These rocks also contain an abundance of quartz and feldspar with few clay minerals. XRD data also confirm the presence of tremolite mixed with chlorite within the gouge at Site #3. This tremolite is highly weathered and extremely soft.

DISCUSSION

Schroeder (2010) identified serpentine polymorphs, chlorite, and “mixed clays” within the gouges at Site #1 (Location 10) and Site #2 (Location 11). Contrary to Schroeder’s findings (2010), this study found no evidence of serpentine polymorphs in any of the fault gouges northeast of LLV. Additionally, EDS analyses of samples from Site #1 (Table 1) identifies the mixed clays found within the gouge as corrensite, chlorite, and corrensite + chlorite interlayered clays.

Even without serpentine minerals, shearing of Franciscan Assemblage melange has caused dissolution-precipitation reactions to crystallize corrensite at Site #1, which is mineralogically similar to the SAFOD borehole (Schleicher et al., 2012; Moore, 2014). In contrast to the surrounding wall rocks, the gouge at Site #1 is rich in magnesium phyllosilicates, indicating authigenic growth of corrensite (Haines and van der Pluijm, 2012). This gouge is highly fractured, allowing for fluid circulation throughout the gouge. When fault strain fractures the grains, both porosity and volume increase, allowing fluid to flow (Haines and van der Pluijm, 2012; Tesei et al., 2012). The fluid ingress causes chlorite or serpentine recrystallization at depth, forming corrensite in the shallow crust (Schroeder, 2010; Moore, 2014). Fluid flow also increases the rate of clay formation, effectively lowering the coefficient of friction of the fault, resulting in stable sliding behavior (Sibson, 1977; Haines and van der Pluijm, 2012; Janssen et al., 2014). Dislocation glide observed in quartz crystals of this study confirms low-

temperature deformation, as corrensite can crystallize at temperatures as low as 60-80◦C, and 1-3 km in depth (Haines and wander Pluijm, 2012) (Figure 14).

Sites #1, #2, and #3 are all chemically similar, and are within 2 km of each other. Magnesium-rich phyllosilicates found in Site #1 are likely due to the abundance of fractures and veins within this particular gouge. Fractures allow for a greater amount of fluid ingress, enhancing the rate of mineral alteration at depth (Tesei et al., 2012; Schleicher et al., 2015). This can be seen in the density of calcite veins and iron oxide stains within the particular gouges. Table 3 summarizes the relationship between fracture density, fluid movement, and the presence of magnesium phyllosilicates within the three gouges in this study. Fluid ingress of each of these gouges is indicated by the density of calcite veins.

Table 3: Summary of the relationship between fracture density, density of calcite veining, and presence of various magnesium phyllosilicates at the three gouges studied.

	Fracture density	**Density of calcite veins**	**Mg-phyllosilicates**
Site #1	High	High	Corrensite Corrensite + Chlorite Chlorite
Site #2	Low	Low	Chlorite
Site #3	Low	Low	Chlorite

Although the gouge at Site #2 is devoid of any significant magnesium-rich clay minerals, the gouge is mineralogically similar to and is on strike with other faults toward the south, such as the East Willits Fault (Schroeder, 2010; Prentice et al., 2014) (Figure 2). Chlorite is present in the gouge, but corrensite is absent. The lack of authigenic corrensite at Site #2 could be the result of lower fluid activity in the gouge. This is supported by the lower fracture and calcite vein density at Site #2. Additionally, the wall rocks at Site #2 are nearly identical to the composition of the fault gouge. Haines and van der Pluijm (2012) noted that a gouge that is mineralogically similar to the surrounding wall rocks is one formed purely by cataclasis. Additionally, the lack of alteration products within the gouges at Sites #2 and #3 may indicate younger faults, as part of the developing upward-facing flower structure centered under LLV (Erickson, 2008). Since this region also contains Franciscan Assemblage blocks with serpentinite lenses at depth, fluid circulation may bring more clay minerals to the surface with time.

Chlorite is found in the surrounding greywacke at Sites #2 and #3, but no authigenic chlorite was found within fractures, as it is at Site #1. Although not an expanding clay, chlorite is a magnesium phyllosilicate and its formation along a fault plane may have implications for aseismic activity (Tesei et al., 2012). First of all, chlorite may recrystallize into corrensite in the shallow crust. As these fault gouges develop, increased fluid content or pressure-temperature conditions could recrystallize the chlorite into corrensite or saponite (Tesei et al., 2012). Corrensite forms at SAFOD at around 200ºC and 2-3 km depth (Schleicher,

2012; Moore, 2014). Secondly, since deformation in phyllosilicate-rich samples is accommodated by frictional and grain-to-grain sliding within the crystal structure of clays, any phyllosilicate may reduce the coefficient of friction for a fault, including chlorite (Haines and van der Pluijm, 2012; Tesei et al., 2012).

Lastly, besides mineralogical evidence, geomorphic evidence also points to movement on faults on the northeast of LLV (Schroeder, 2010). Schroeder (2010) noted evidence of a Pleistocene landslide at Site #2. Also, sites #1 and #3 are only about 500 m apart, yet represent entirely different drainage systems. In contrast to the drainage divides outlined by Erickson (2008), Site #1 drains toward String Creek in the east and ultimately into the Russian River south of Willits. Site #3 drains west into LLV, eventually draining into the Eel River north of Willits.

CONCLUSION

Although the presence of serpentine minerals within these three gouges could not be confirmed, XRD and SEM analyses confirmed that both corrensite and corrensite + chlorite are in the fault gouge at Site #1, providing the potential evidence that the faults in this investigation may be creeping, accommodating some of the strain on the MFZ (Moore, 2014; Prentice et al., 2014; Schleicher et al., 2015). Site #1 has extensive fractures allowing for fluid flow, which would produce favorable paragenetic conditions for the formation of corrensite. Calcite veins and abundant iron oxides in this gouge provide further evidence for fluids as an important factor in the development of the phyllosilicate assemblage, especially corrensite. The presence of magnesium-rich phyllosilicates within gouges of Franciscan Assemblage melange material at Site #1 supports the hypothesis that it is creeping. This aseismic behavior decreases the overall strain on the MFZ and the potential future seismic hazard of the region (Prentice et al., 2014).

The lack of any saponite clay minerals at Sites #2 and #3 could be due to several possible factors. Both of these fault gouges had few, if any, fractures for fluid flow within the gouge. Additionally, the fault gouge itself was mineralogically similar to the surrounding wall rocks, indicating younger faults (Haines and van der Pluijm, 2012). The lack of fractures at Sites #2 and #3 may restrain fluid flow from within the gouge, not allowing clay crystallization. However, these faults are on strike with other creeping faults toward the south, which are also within the

MFZ (Schroeder, 2010). These faults all have the same protolith, which includes large serpentinite lenses below LLV (Schroeder, 2010). Over time, serpentine recrystallization beneath LLV may eventually develop magnesium-rich phyllosilicates within these faults. Expanding saponite clays within these gouges would increase pore pressure within the gouge, allowing for greater fluid movement, and increased rates of recrystallization.

In the absence of a survey, current aseismic movement along the northeastern fault segments of the MFZ cannot be confirmed. However, strain accumulation on this developing fault system is likely being accommodated by a wide region of faults in the system through creep, reducing the seismic hazard of the MFZ. With many young faults within a developing system, this region would further benefit from a thorough geologic mapping, focused on locating other faults within this zone. Further research in this region would also include electron microprobe analysis to obtain quantitative chemical analyses for clays and other minerals in fault gouges on a wide range of faults within the MFZ.

REFERENCES

Bilham, R. and P. Bodin, 1992, Fault zone connectivity: Slip rates on faults in the San Francisco Bay Area, California: Science, v. 258, no. 5080, p. 281-284.

Bradbury, K.K., D.C. Barton, J.G. Solum, S. D. Draper, and J. P. Evans, 2007, Mineralogic and textural analyses of drill cuttings from the San Andreas Fault Observatory at Depth (SAFOD) boreholes: Initial interpretations of fault zone composition and constraints on geologic models: Geosphere, v. 3, no. X.

Brigatti, M.F., E. Galan, and B.K.G. Theng, 2013, Structure and mineralogy of clay minerals: Developments in Clay Science, v. 5A.

Carpenter, B.M., D.M. Saffer, and C. Marone, 2012, Frictional properties and sliding stability of the San Andreas Fault from deep drill core: Geology, v. 40, no. 8, p.759-762.

Erickson, G., 2008, Evolution of an intermontane basin along the Maacama Fault, Little Lake Valley, Northern California [Master of Science thesis]: Humboldt State University, Arcata, 121 p.

Evans, B. W., K. Hattori, and A. Baronnet, 2013, Serpentinite: What, why, where?: Elements, v. 9, p. 99-106.

Festa, A., G. A. Pini, Y. Dilek, and G. Codegone, 2010, Melanges and melange-forming processes: a historical overview and new concepts: International Geology Review, v. 52, no., 10-12, p. 1040-1105.

Funning, G. J., R. Burgmann, A. Ferretti, F. Novali, and A. Fumagalli, 2007, Creep on the Rodgers Creek Fault, northern San Francisco Bay Area from a 10 year PS-InSAR dataset: Geophysical Research Letters, v. 34.

Galehouse, J.S. and James J. Lienkaemper, 2003, Inferences drawn from two decades of alinement array measurements of creep on faults in the San Francisco Bay Region, v. 93, no. 6, p. 2415-2433.

Guillot, S., S. Schwartz, B. Reynard, P. Agard, and C. Prigent, 2015, Tectonic significance of serpentinites: Tectonophysics, Article in press.

Haines, S. H., and B. van der Pluijm, 2012, Patterns of mineral transformations in clay gouge, with examples from low-angle normal fault rocks in the Western USA: Journal of Structural Geology, v. 43, p. 2-32.

Harris, R., 2017, Large earthquakes and creeping faults: Reviews of Geophysics, v. 55, p. 169-198.

Herd, D. G., 1978, Intercontinental plate boundary east of Cape Mendocino, California: Geology, v. 6, p. 721-725.

Janssen, C., R. Wirth, H.-R. Wenk, L. Morales, R. Naumann, M. Kienast, S.-R. Song, and G. Dresen, 2014, Faulting processes in active faults—evidences from TCDP and SAFOD drill core samples: Journal of Structural Geology, v. 65, p. 100-116.

Jouanne, F., F. A. Audemard, C. Beck, A. Van Welden, R. Ollarves, and C. Renioza, 2011, Present-day deformation along the El Pilar Fault in Eastern Venezuela: Evidence of creep along a major transform boundary: Journal of Geodynamics, v. 51, p. 398-410.

Hsu, K. J., 1968, Principles of melanges and their bearing on the Franciscan-Knoxville Paradox, Geological Society of America Bulletin, v. 79, p. 1063-1074.

Koehler, R. D., R. C. Witter, G. D. Simpson, and E. Hemphill-Haley, 2005, Paleoseismic Investigation of the Northern San Gregorio Fault, Half Moon Bay, California, final technical report, U.S. Geological Survey National Earthquake Hazards Reduction Program, Award #04HQGR0045.

McLaughlin, R.E., M.C. Blake, Jr., A. Griscom, 1988, Tectonics for formation, translation, and dispersal of the Coast Range Ophiolite of California: Tectonics, v. 7, no. 5, p. 1033-1056.

Moore, D. E., 2014, Comparative mineral chemistry and textures of SAFOD fault gouge and damage-zone rocks: Journal of Structural Geology, v. 68, p. 82-96.

Moore, D. E. and D. A. Lockner, 2007, Comparative deformation behavior of minerals in serpentinized ultramafic rock: Applications to the slab-mantle interface in subduction zones: International Geology Review, v. 49, p. 401-415.

Moore, D. E. and D. A. Lockner, 2013, Chemical controls on fault behavior: Weakening of serpentinite sheared against quartz-bearing rocks and its significance for fault creep in the San Andreas System: Journal of Geophysical Research: Solid Earth, v.118, p. 1-13.

Moore, D. E. and M. J. Rymer, 2007, Talc-bearing serpentinite and the creeping section of the San Andreas Fault: Letters to Nature, v. 448.

Moore, D. E. and M. J. Rymer, 2012, Correlation of clayey gouge in a surface exposure of serpentinite in the San Andreas Fault with gouge from the San Andreas Fault Observatory at Depth (SAFOD): Journal of Structural Geology, v. 38, p. 51-60.

Murakami, T., T. Sato, and A. Inoue, 1999, HRTEM evidence for the process and mechanism of saponite-to-chlorite conversion through corrensite: American Mineralogist, v. 84, p. 1080-1087.

Murray, J. R., S. E. Minson, and J. L. Svarc, 2014, Slip rates and spatially variable creep on faults of the northern San Andreas System inferred through Bayesian inversion of Global Positioning System data: Journal of Geophysical Research: Solid Earth, v. 119, p. 6023-6047.

Prentice, C. S., M. C. Larsen, H. M. Kelsey, and J. Zachariasen, 2014, Late Holocene slip rate and ages of prehistoric earthquakes along the Maacama Fault near Willits, Mendocino County, Northern California: Bulletin of the Seismological Society of America, v. 104, n. 6.

Schedl, A. and B. A. van der Pluijm, 1988, A review of deformation microstructures: Journal of Geological Education, v. 36, n. 2.

Schleicher, A.M., B.A. van der Pluijm, and L.N. Warr, 2012, Chlorite-smectite clay minerals and fault behavior: New evidence from the San Andreas Fault Observatory at Depth (SAFOD) core: Lithosphere, v. 4, n. 3, p. 209-220.

Schleicher, A.M., R. Sutherland, J. Townend, V.G. Toy, and B.A. van der Pluijm, 2015, Clay mineral formation and fabric development in the DFDP-1B borehole, central Alpine Fault, New Zealand: New Zealand Journal of Geology and Geophysics, v. 58, no. 1, 13-21.

Schroeder, R. D., 2010, Kinematic evolution of the Maacama Fault Zone, Northern California Coast Ranges [Ph.D. thesis]: University of Calgary, Calgary, Alberta, 203 p.22.

Shau, Yen-Hong, D.R. Peacor, and E.J. Essene, 1990, Corrensite and mixed-layer chlorite/corrensite in metabasalt from northern Taiwan: TEM/AEM, EMPA, XRD, and optical studies: Contributions to Mineralogy and Petrology, v. 105, p. 123-142.

Sibson, R.H., 1977, Fault rocks and fault mechanisms: Journal of the Geological Society of London, v. 133, p. 191-213.

Sone, H., T. Shimamoto, and D. E. Moore, 2012, Frictional properties of saponite-rich gouge from a serpentinite-bearing fault zone along the Gokasho-Arashima Tectonic Line, central Japan: Journal of Structural Geology, v. 38, p. 172-182.

Tesei, T., C. Collettini, B. M. Carpenter, C. Viti, and C. Marone, 2012, Frictional strength and healing behavior of phyllosilicate-rich faults: Journal of Geophysical Research, v. 117.

Wakabayashi, J., 1992, Nappes, tectonics of oblique plate convergence, and metamorphic evolution related to 140 million years of continuous subduction, Franciscan Complex, California, Journal of Geology, v. 100, n. 1, p. 19-40.

Wakabayashi, J., 1999, Subduction and the rock record: concepts developed in the Franciscan Complex, California, Geological Society of America Special Paper, 338.

Woolace, A. C., 2005, Late Neogene and Quaternary Stratigraphy and Structure of Little Lake Valley, Northern Coast Range, California [Master of Science thesis]: Humboldt State University, Arcata, 67 p.